

Quantum Ising chains with boundary fields

Massimo Campostrini¹, Andrea Pelissetto² and Ettore Vicari¹

¹ Dipartimento di Fisica dell'Università di Pisa and INFN, Sezione di Pisa, I-56127 Pisa, Italy

² Dipartimento di Fisica di Sapienza, Università di Roma and INFN, Sezione di Roma I, Piazzale A. Moro 2, I-00185 Roma, Italy

E-mail: `campo@df.unipi.it`, `Andrea.Pelissetto@roma1.infn.it`,
`Ettore.Vicari@df.unipi.it`

Abstract. We present a detailed study of the finite one-dimensional quantum Ising chain in a transverse field in the presence of boundary magnetic fields coupled with the order-parameter spin operator. We consider two magnetic fields located at the boundaries of the chain that have the same strength and that are aligned in the same or in the opposite direction. We derive analytic expressions for the gap in all phases for large values of the chain length L , as a function of the boundary field strength. We also investigate the behavior of the chain in the quantum ferromagnetic phase for oppositely aligned fields, focusing on the magnet-to-kink transition that occurs at a finite value of the magnetic field strength. At this transition we compute analytically the finite-size crossover functions for the gap, the magnetization profile, the two-point correlation function, and the density of fermionic modes. As the magnet-to-kink transition is equivalent to the wetting transition in two-dimensional classical Ising models, our results provide new analytic predictions for the finite-size behavior of Ising systems in a strip geometry at this transition.

1. Introduction

The quantum Ising chain is a useful theoretical laboratory in which fundamental issues concerning quantum many-body systems can be thoroughly investigated, exploiting the exact knowledge of several features of its phase diagram and quantum correlations. Many results for its low-energy properties have been derived in the quantum ordered and disordered phases, and, in particular, at the quantum critical point separating the two phases, both in the thermodynamic limit and in the finite-size scaling (FSS) limit with several types of boundary conditions, see, e.g., Refs. [1, 2, 3, 4, 5, 6, 7, 8, 9, 10, 11, 12, 13, 14, 15, 16, 17, 18, 19, 20, 21, 22, 23] and references therein.

In this paper we extend these analytic results to the case in which boundary fields are present. We present a detailed study of the quantum Ising chain in a transverse magnetic field [5] in the presence of magnetic fields coupled with the order-parameter spin operator, located at the boundaries of the chain. We assume the two magnetic fields to have the same strength and consider two cases: (i) the two fields are parallel; (ii) the two fields are oppositely aligned. As expected, in the quantum paramagnetic phase the boundary fields do not change the large-size behavior of low-energies quantities. At the critical point, bulk behavior is independent of boundary conditions. However, the magnetic fields induce a surface phase transition with a corresponding scaling behavior. The quantum ferromagnetic phase is more interesting. If the boundary fields have opposite direction, one observes two different bulk phases. For small magnetic fields, the ground state is ferromagnetic as it occurs in the absence of boundary interactions. On the other hand, kink states [1] are the relevant low-energy excitations for large boundary fields. The two different phases are separated by a continuous transition that is only characterized by the nature of the two coexisting phases and, indeed, the same transition occurs in Ising rings in the presence of a localized link defect [23].

Because of the quantum-to-classical mapping, our results can also be applied to the two-dimensional Ising model, and, more generally, to any model in the Ising universality class, in a strip geometry. In the two-dimensional case the quantum transition between the ferromagnetic and the kink phase corresponds to the wetting transition, which, in the context of a strip geometry, is sometimes identified as an interface localization/delocalization transition [24, 25, 26, 27]. Our results, therefore, provide new analytic expressions for two-dimensional Ising systems at the wetting transition in the presence of boundary magnetic fields.

The paper is organized as follows. In Sec. 2 we introduce the one-dimensional quantum Ising chain with boundary fields. In Sec. 3 we compute the low-energy spectrum by exploiting the equivalent quadratic fermionic formulation of the Hamiltonian [3, 5]. Explicit calculations are reported in the following sections. Secs. 4, 5 and 6 report results for the quantum paramagnetic phase, at the quantum critical point and for the ordered magnetized phase, respectively. Sec. 7 is devoted to the study of the magnet-to-kink transition driven by the boundary fields in the ordered phase. We obtain exact results for the gap, the magnetization profile, the two-point spin-spin correlation

function, and the entanglement entropy. In Sec. 7.5 these results are compared with the existing ones for two-dimensional classical models. Finally, in Sec. 8 we summarize the main results and draw our conclusions. A number of appendices report the derivations of some of the results.

2. Model and definitions

The Hamiltonian of the quantum Ising chain in a transverse magnetic field is given by

$$H = -J \sum_{i=1}^{L-1} \sigma_i^{(1)} \sigma_{i+1}^{(1)} - g \sum_{i=1}^L \sigma_i^{(3)}, \quad (1)$$

where $\sigma^{(i)}$ are the Pauli matrices. In the following we assume ferromagnetic nearest-neighbor interactions with $J = 1$, and $g > 0$.

The Ising chain undergoes a continuous transition at $g = 1$ [5], separating a quantum ferromagnetic phase ($g < 1$) from a quantum paramagnetic phase ($g > 1$). In this paper we investigate the effects of boundary magnetic fields aligned along the x axis. They give rise to an additional energy term

$$H_b = -\zeta_1 \sigma_1^{(1)} - \zeta_L \sigma_L^{(1)} \quad (2)$$

that is added to Hamiltonian (1). In the following we shall consider the model in the specific case of equal parallel boundary fields (PBF)

$$\zeta_L = \zeta_1 = \zeta, \quad (3)$$

and of equal oppositely-aligned boundary fields (OBF)

$$\zeta_L = -\zeta_1 = \zeta. \quad (4)$$

It is not restrictive to assume $\zeta > 0$ in both cases.

We will often use a basis in which $\sigma_i^{(1)}$ is diagonal. States will be labelled as $|s_1, s_2, \dots, s_L\rangle$, where s_i is the eigenvalues of $\sigma_i^{(1)}$. Signs will be fixed so that $\sigma_i^{(3)}$ has the form

$$\sigma_i^{(3)} = \begin{pmatrix} 0 & 1 \\ 1 & 0 \end{pmatrix} \quad (5)$$

in this basis. In the absence of boundary fields, the Hamiltonian commutes with the generator $P_z = \prod_i \sigma_i^{(3)}$ of the \mathbb{Z}_2 transformations $|s\rangle \rightarrow -|s\rangle$ and with the operator T of the reflection transformations defined by $T|s_1, s_2, \dots, s_L\rangle = |s_L, s_{L-1}, \dots, s_1\rangle$. These operators do not generally commute with H_b . However, note that $[P_z T, H_b] = 0$ for OBF.

In this paper we analyze the low-energy spectrum of the model. In particular, we compute the energy differences between the lowest states and the ground state

$$\Delta_n \equiv E_n - E_0, \quad \Delta \equiv \Delta_1, \quad (6)$$

(here E_n are the energy eigenvalues ordered so that $E_0 \leq E_1 \leq E_2 \dots$, and Δ is the gap), the local magnetization and the two-point correlation function,

$$m(i) \equiv \langle \sigma_i^{(1)} \rangle, \quad G(i, j) \equiv \langle \sigma_i^{(1)} \sigma_j^{(1)} \rangle. \quad (7)$$

For OBF, because of the symmetry under $P_z T$, we have $m(i) = -m(L - i)$ and, as a consequence, the average magnetization $\sum_{i=1}^L m(i)$ always vanishes. We also define the integrated correlation χ and the correlation length ξ with respect to the center of the chain:

$$\chi = \sum_i G(L/2, i), \quad \xi^2 = \frac{1}{2\chi} \sum_i (i - L/2)^2 G(L/2, i). \quad (8)$$

3. Jordan-Wigner representation and Hamiltonian diagonalization

3.1. Fermionic representation

To determine the spectrum of Hamiltonian (1), we extend the model, considering two additional spins located in 0 and $L + 1$ and the Hamiltonian

$$H_e = -J \sum_{i=1}^{L-1} \sigma_i^{(1)} \sigma_{i+1}^{(1)} - J_0 \sigma_0^{(1)} \sigma_1^{(1)} - J_L \sigma_L^{(1)} \sigma_{L+1}^{(1)} - g \sum_{i=1}^L \sigma_i^{(3)}. \quad (9)$$

This is the Ising Hamiltonian with two different couplings on the boundary links and zero transverse field on the boundaries. Let us note that the Hamiltonian H_e commutes with both $\sigma_0^{(1)}$ and $\sigma_{L+1}^{(1)}$, which can therefore be simultaneously diagonalized. The Hilbert space can be divided into four sectors, which we label as $(1, 1)$, $(-1, 1)$, $(1, -1)$ and $(-1, -1)$, where (s_0, s_{L+1}) are the eigenvalues of $\sigma_0^{(1)}$ and $\sigma_{L+1}^{(1)}$. The restriction of H_e to each sector gives rise to the Hamiltonian H , defined in Eq. (1), with a boundary term of the form (2). Hence, the spectrum of H_e also provides the spectrum of $H + H_b$. Let us also note that H_e is \mathbb{Z}_2 symmetric. Indeed, if $P_z = \prod_{i=0}^{L+1} \sigma_i^{(3)}$, then $[H_e, P_z] = 0$. Since P_z does not commute with $\sigma_0^{(1)}$ and $\sigma_{L+1}^{(1)}$, the spectrum is necessarily degenerate. Moreover, since P_z anticommutes with these two boundary operators, P_z maps sector $(1, 1)$ to $(-1, -1)$ and $(1, -1)$ to $(-1, 1)$, so that the restriction of H_e to $(1, \pm 1)$ allows us to compute the full spectrum of H_e .

To compute the spectrum of Hamiltonian (9), we follow Ref. [3]. We first perform a Jordan-Wigner transformation, defining fermionic operators c_i and c_i^\dagger

$$c_i^\dagger = R_i \sigma_i^+, \quad c_i = \sigma_i^- R_i, \quad R_i = (-1)^{i-1} \prod_{j=1}^{i-1} \sigma_j^{(3)}, \quad (10)$$

where $\sigma^\pm = (\sigma^{(1)} \pm \sigma^{(2)})/2$. These relations can be inverted, obtaining

$$\sigma_i^{(1)} = R_i (c_i^\dagger + c_i), \quad \sigma_i^{(3)} = 2c_i^\dagger c_i - 1. \quad (11)$$

Thus, Hamiltonian (9) becomes

$$H_e = -g \sum_{i=1}^L (2c_i^\dagger c_i - 1) - \sum_{i=0}^L J_i (c_i^\dagger c_{i+1} + c_{i+1}^\dagger c_i + c_i^\dagger c_{i+1}^\dagger + c_{i+1} c_i), \quad (12)$$

with $J_i = J = 1$ for $i = 1, \dots, L-1$. In this formalism $\sigma_0^{(1)} = c_0 + c_0^\dagger$ and $\sigma_{L+1}^{(1)} = P_z(c_{L+1}^\dagger - c_{L+1})$. To go further, let us rewrite H_e as

$$H_e = Lg - \sum_{i,j=0}^{L+1} \left[c_i^\dagger A_{ij} c_j + \frac{1}{2} c_i^\dagger B_{ij} c_j^\dagger + \frac{1}{2} c_i B_{ij} c_j \right], \quad (13)$$

with A and B symmetric and antisymmetric matrices, respectively. Then, we perform a Bogoliubov transformation. We introduce new canonical fermionic variables

$$\eta_k = \sum_{i=0}^{L+1} (g_{ki} c_i^\dagger + h_{ki} c_i), \quad (14)$$

where g_{ki} and h_{ki} are fixed by the requirement that H takes the form

$$H_e = E_{gs} + \sum_{k=0}^{L+1} \mathcal{E}_k \eta_k^\dagger \eta_k, \quad (15)$$

with $0 \leq \mathcal{E}_0 \leq \mathcal{E}_1 \leq \dots$. Following Ref. [3], we define the vectors

$$U_k = (g_{k0} + h_{k0}, g_{k1} + h_{k1}, \dots), \quad V_k = (g_{k0} - h_{k0}, g_{k1} - h_{k1}, \dots). \quad (16)$$

The variables η_k satisfy canonical anticommutation relations if the vectors U_k form an orthonormal basis, and so does the set V_k . The vectors V_k satisfy

$$(A+B)(A-B)V_k = \mathcal{E}_k^2 V_k, \quad (17)$$

which turns the determination of the energies \mathcal{E}_k into an eigenvalue problem. If \mathcal{E}_k does not vanish, U_k is given by

$$U_k = \frac{1}{\mathcal{E}_k} (A-B)V_k. \quad (18)$$

If \mathcal{E}_k is zero, U_k is the null eigenvector of $(A-B)(A+B)$. It is also possible to evaluate the constant E_{gs} in Eq. (15), which provides the energy of the ground state:

$$E_{gs} = -\frac{1}{2} \sum_{k=0}^{L+1} \mathcal{E}_k. \quad (19)$$

The matrix $C = \frac{1}{4}(A+B)(A-B)$ is given by (we write the 5×5 matrix C for $L=3$, the generalization to any L being obvious)

$$C = \begin{pmatrix} J_0^2 & gJ_0 & 0 & 0 & 0 \\ gJ_0 & 1+g^2 & g & 0 & 0 \\ 0 & g & 1+g^2 & g & 0 \\ 0 & 0 & g & J_L^2 + g^2 & 0 \\ 0 & 0 & 0 & 0 & 0 \end{pmatrix}. \quad (20)$$

This matrix C has a zero eigenvalue, $\mathcal{E}_0 = 0$, with eigenvector $V_0 = (0, \dots, 0, 1)$. Correspondingly, we obtain $U_0 = (1, 0, \dots, 0)$ and

$$\eta_0 = \frac{1}{2}(c_0 + c_0^\dagger) + \frac{1}{2}(c_{L+1}^\dagger - c_{L+1}) = \sigma_0^{(1)} + (-1)^L P_z \sigma_{L+1}^{(1)} \quad (21)$$

which depends only on the boundary fermion operators. Note that it can be rewritten as a combination of $\sigma_0^{(1)}$, $\sigma_{L+1}^{(1)}$, and P_z , hence it does not represent an additional symmetry of the Hamiltonian. The presence of a zero eigenvalue was expected, as the spectrum is degenerate. If J_0 and J_L do not vanish, since there is only one fermion operator with zero energy, the spectrum is doubly degenerate.

Let us now consider the nonzero eigenvalues. Since the vectors V_k are an orthonormal set, orthogonality with V_0 implies $V_k = (a_0, \dots, a_L, 0)$. It follows analogously $U_k = (0, b_1, \dots, b_{L+1})$. Therefore, we have for $k = 1, \dots, L+1$

$$\eta_k = \frac{a_0}{2}(c_0^\dagger - c_0) + \frac{b_{L+1}}{2}(c_{L+1} + c_{L+1}^\dagger) + \dots \quad (22)$$

where the dots represent a polynomial in c_j and c_j^\dagger with $1 \leq j \leq L$. It is then easy to verify that

$$\{\eta_k, \sigma_0^{(1)}\} = [\eta_k, \sigma_{L+1}^{(1)}] = 0. \quad (23)$$

It follows that, if a state $|\psi\rangle$ satisfies $\sigma_0^{(1)}|\psi\rangle = s_0|\psi\rangle$, then we have $\sigma_0^{(1)}\eta_k|\psi\rangle = -s_0\eta_k|\psi\rangle$. Analogously, if $\sigma_{L+1}^{(1)}|\psi\rangle = s_{L+1}|\psi\rangle$, we have $\sigma_{L+1}^{(1)}\eta_k|\psi\rangle = s_{L+1}\eta_k|\psi\rangle$. Therefore, if $|\psi\rangle$ belongs to sector (s_0, s_{L+1}) , then $\eta_k|\psi\rangle$ belongs to sector $(-s_0, s_{L+1})$.

To conclude, we should determine to which sectors the two degenerate ground states belong. If J_0 and J_L are both positive, we expect the ground-state configurations to be ordered. Therefore, if on one boundary the spin is directed in the positive x direction, we expect the same to occur at the other end of the chain. Therefore, we conclude that the ground states belong to sectors $(+1, +1)$ and $(-1, -1)$. This identification is supported by exact diagonalization.

We can now classify the states. We only consider the states with $s_0 = +1$, to avoid the double degeneracy. Then, if $J_0, J_L > 0$ we have:

- 1) In the sector $s_0 = 1, s_{L+1} = 1$, the lowest energy state is the ground state of the Hamiltonian and all states are obtained as $\eta_{k_1}^\dagger \dots \eta_{k_m}^\dagger |0\rangle$, $k_i \geq 1$, with m even. The first excited state is $\eta_2^\dagger \eta_1^\dagger |0\rangle$ and the energy gap is $\Delta = \mathcal{E}_1 + \mathcal{E}_2$.
- 2) In the sector $s_0 = 1, s_{L+1} = -1$, the lowest energy state is the first excited state $\eta_1^\dagger |0\rangle$ of the Hamiltonian H_e and all states are obtained as $\eta_{k_1}^\dagger \dots \eta_{k_m}^\dagger |0\rangle$, $k_i \geq 1$, with m odd. In particular, the first excited state in the sector is $\eta_2^\dagger |0\rangle$, so that the energy gap is $\Delta = \mathcal{E}_2 - \mathcal{E}_1$.

The first case is relevant when considering $\zeta_1, \zeta_L > 0$ in the boundary Hamiltonian H_b , which are identified with J_0 and J_L , respectively. The second case is relevant when ζ_1 and ζ_L have opposite signs: the corresponding gap is obtained by identifying $\zeta_1 = J_0$ and $\zeta_L = -J_L$.

3.2. Exact results for the energy gap

The energy spectrum of Hamiltonian H_e can be computed exactly, as discussed in Appendix A. Here we will focus on the case $J_0 = J_L = \zeta$, which allows us to derive the

spectrum for parallel or opposite equal magnetic fields at the boundary, cf. Eqs. (3) and (4), respectively. Neglecting the irrelevant zero eigenvalue, we obtain $L + 1$ elementary excitations whose energy \mathcal{E}_m is given by

$$\mathcal{E}_m = 2\sqrt{1 + g^2 - 2g \cos k_m}, \quad (24)$$

where k_m are the $L + 1$ solutions of the equation

$$\begin{aligned} [(1 + g^2)(1 - 2\zeta^2) + \zeta^4 - 2g \cos k(1 - \zeta^2)^2] \sin kL = \\ g(1 - 2g \cos k + g^2 - \zeta^4) \sin[k(L + 1)]. \end{aligned} \quad (25)$$

We should consider real solutions in $[0, \pi[$ (correspondingly $|1 - g| \leq \mathcal{E}_m \leq 1 + g$), purely imaginary solutions $k = ih$ with $h > 0$ (correspondingly $\mathcal{E}_m < |1 - g|$), and solutions $k = \pi + ih$ (correspondingly $\mathcal{E}_m > 1 + g$). Equation (25) has also a spurious solution for $k = 0$ for all values of the parameters, which should be discarded. For $g = 1 - \zeta^2$, there is also a second solution with $k = 0$, which corresponds to a true excitation of the model. For $\zeta = 0$ we obtain the equation appropriate for open boundary conditions (OBC) [5],

$$\frac{\sin k(L + 1)}{\sin kL} = \frac{1}{g}, \quad (26)$$

and $1 + g^2 - 2g \cos k = 0$, which implies an additional zero mode for H_e . This is not surprising as the spectrum has a fourfold degeneracy for $J_0 = J_L = 0$: the four sectors are equivalent in the absence of boundary fields.

The real solutions of Eq. (25) are obtained by solving

$$\tan kL = \frac{g \sin k(1 + g^2 - \zeta^4 - 2g \cos k)}{(1 - \zeta^2)^2 + g^2(1 - 2\zeta^2) - g[g^2 - 1 + (2 - \zeta^2)^2] \cos k + 2g^2 \cos^2 k}. \quad (27)$$

The imaginary solutions are obtained by setting $k = ih$. Eq. (25) then becomes

$$e^{2hL} = \frac{e^{-h}(e^h g - 1)[e^h(1 - \zeta^2) - g]^2}{(g - e^h)(e^h g - 1 + \zeta^2)^2}. \quad (28)$$

The corresponding energies $\mathcal{E} = 2\sqrt{1 + g^2 - 2g \cosh h}$ are always smaller than those corresponding to real momenta, hence the localized states are the most important ones in the determination of the low-energy spectrum.

4. The quantum paramagnetic case

For $g > 1$ (paramagnetic phase) the lowest energy state is a localized state, i.e., a solution of Eq. (28) with $h > 0$. For large values of L we must consider the poles in the right-hand side of the equation. They are

$$e^h = g, \quad e^h = \frac{1 - \zeta^2}{g}. \quad (29)$$

For $g > 1$, the second equation does not have any solution. The relevant pole is the first one, so that the relevant solution can be written as $e^h = g + \epsilon$. For large values of L , substituting this expression in Eq. (28), we obtain

$$\epsilon = -\frac{\zeta^4 g(g^2 - 1)}{(g^2 - 1 + \zeta^2)^2} g^{-2L}. \quad (30)$$

Correspondingly, we find

$$\mathcal{E}_1 = 2\frac{\zeta^2(g^2 - 1)}{(g^2 - 1 + \zeta^2)} g^{-L}. \quad (31)$$

The energy \mathcal{E}_1 vanishes with exponentially small corrections. The energy of the second excited state corresponds to the lowest value k_{\min} of k satisfying Eq. (27). We obtain $k_{\min} = \pi/L + O(L^{-2})$ and

$$\mathcal{E}_2 = 2(g - 1) + \frac{g\pi^2}{g - 1} \frac{1}{L^2} + O(L^{-3}). \quad (32)$$

The system is therefore gapped, and the same gap is obtained for both PBF and OBF modulo exponentially small corrections, since $\mathcal{E}_2 - \mathcal{E}_1 \approx \mathcal{E}_2 + \mathcal{E}_1 + O(g^{-L})$:

$$\Delta = 2(g - 1) + \frac{g\pi^2}{g - 1} \frac{1}{L^2} + O(L^{-3}). \quad (33)$$

Note that the same result would have been obtained for OBC, confirming that boundary conditions and/or boundary fields are irrelevant in the paramagnetic quantum phase.

5. Critical-point behavior

5.1. Finite-size scaling for $g = 1$

At the critical point $g = 1$, there are no localized solutions, hence the two lowest energies \mathcal{E}_n are obtained by considering Eq. (27). The equation becomes

$$\tan kL = \frac{\cot(k/2)(\zeta^4 - 4\sin^2 k/2)}{4\zeta^2 - \zeta^4 - 4\sin^2 k/2}. \quad (34)$$

The lowest-energy solutions correspond to momenta that scale as $k \sim 1/L$. Therefore, we can expand the right-hand side in powers of k , obtaining

$$\tan kL = \frac{2\zeta^2}{4 - \zeta^2} \frac{1}{k} + O(k), \quad (35)$$

which shows that $\tan kL$ must diverge for $L \rightarrow \infty$. This fixes $k_n \approx (n - 1/2)\pi/L$ with $n = 1, 2, \dots$. Including the corrections, we obtain for the two lowest momenta

$$k_1 = \frac{\pi}{2L} + \frac{\pi}{L^2} \frac{\zeta^2 - 4}{4\zeta^2}, \quad k_2 = \frac{3\pi}{2L} + \frac{3\pi}{L^2} \frac{\zeta^2 - 4}{4\zeta^2}, \quad (36)$$

so that

$$\mathcal{E}_1 = \frac{\pi}{L} + \frac{\pi}{L^2} \frac{\zeta^2 - 4}{2\zeta^2}, \quad \mathcal{E}_2 = \frac{3\pi}{L} + \frac{3\pi}{L^2} \frac{\zeta^2 - 4}{2\zeta^2}. \quad (37)$$

These results imply that the PBF and OBF gaps are

$$\Delta_{\text{PBF}} = \frac{4\pi}{L} + \frac{2\pi}{L^2} \frac{\zeta^2 - 4}{\zeta^2}, \quad (38)$$

$$\Delta_{\text{OBF}} = \frac{2\pi}{L} + \frac{\pi}{L^2} \frac{\zeta^2 - 4}{\zeta^2}, \quad (39)$$

respectively. Note that the amplitude of the $1/L$ term differs from that obtained in the OBC case (corresponding to $\zeta = 0$) [5],

$$\Delta_{\text{OBC}} = \frac{\pi}{L} + O(L^{-2}), \quad (40)$$

indicating that $\zeta = 0$ is a surface critical point.

As we have discussed in Ref. [21] in the OBC case, the corrections of order $1/L$ to the leading behavior can be interpreted as the effect of a nonlinear scaling field associated with L : the leading irrelevant boundary operator gives corrections that scale as L^{-2} . The same holds in the presence of boundary fields. Indeed, we can define a new length scale L_{eff} so that

$$\Delta_{\text{PBF}} = \frac{4\pi}{L_{\text{eff}}} + O(L_{\text{eff}}^{-3}), \quad \Delta_{\text{OBF}} = \frac{2\pi}{L_{\text{eff}}} + O(L_{\text{eff}}^{-3}). \quad (41)$$

Using the previously reported expressions we obtain

$$L_{\text{eff}} = L - \frac{1}{2} \frac{\zeta^2 - 4}{\zeta^2}. \quad (42)$$

Note that the same rescaling applies both to PBF and OBF, a result which is not obvious in the original formulation, but which has a natural explanation in the present setting in which we consider H_e . Indeed, the rescaling should cancel the leading correction in the whole low-energy spectrum of H_e , hence in all low-energy excitation energies \mathcal{E}_k . Therefore, it should apply to both PBF and OBF.

Since $\zeta = 0$ is a surface critical point and the boundary term is a relevant perturbation, we can study the crossover behavior close to $\zeta = 0$. The relevant scaling variable is $\zeta_b = \zeta L^{1/2}$. Therefore, in the limit $\zeta \rightarrow 0$, $L \rightarrow \infty$ at fixed ζ_b we have

$$\Delta(\zeta, L) = L f_b(\zeta_b), \quad (43)$$

where the function $f_b(\zeta_b)$ depends on the type, OBF or PBF, of boundary fields. In the scaling limit defined above, momenta scale as $k = b/L$. Using Eq. (34), we obtain an implicit equation for b :

$$\tan b = \frac{1}{2b} \frac{\zeta_b^4 - b^2}{\zeta_b^2}. \quad (44)$$

Therefore, to compute the scaling function, one determines the two lowest values of b satisfying Eq. (44) and uses them to determine the gap as before. The scaling curves are reported in Fig. 1.

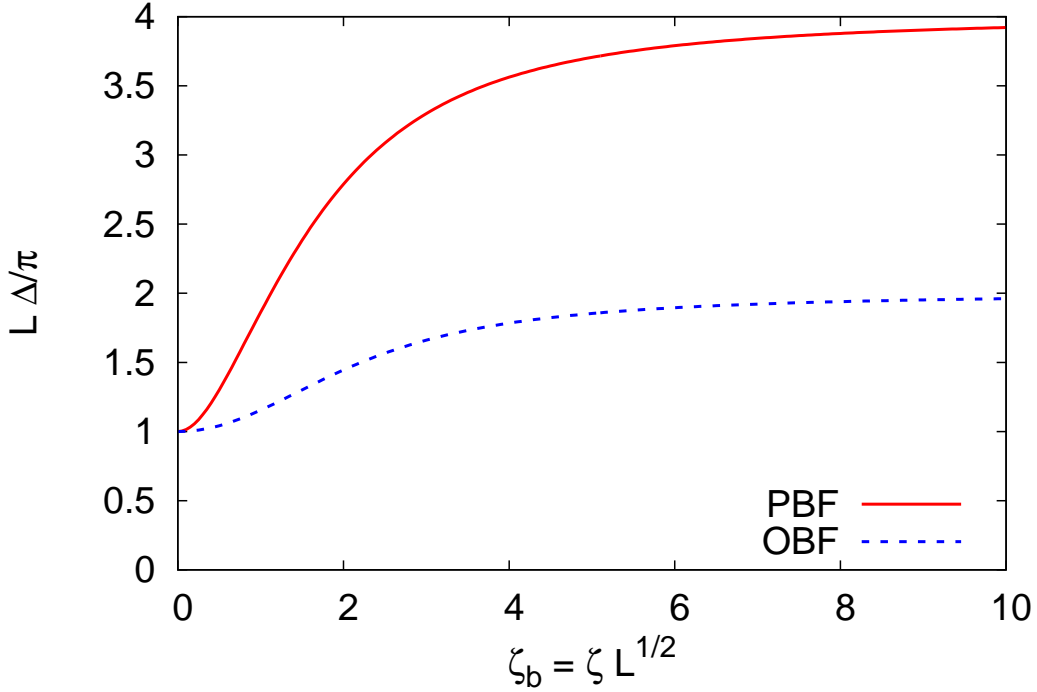


Figure 1. (Color online) Crossover curves for $L\Delta/\pi$ as a function of $\zeta_b = \zeta L^{1/2}$. For $\zeta_b \rightarrow 0$ we recover the OBC case and $L\Delta/\pi \rightarrow 1$. For $\zeta_b \rightarrow +\infty$ we obtain $L\Delta/\pi \rightarrow 2$ for OBF and $L\Delta/\pi \rightarrow 4$ for PBF.

5.2. Scaling behavior close to the critical point

Let us now consider the scaling behavior in a neighborhood of the critical point $g = 1$. The corresponding scaling variable is

$$w = (g - 1)L. \quad (45)$$

The relevant equations are obtained from Eqs. (27) and (28) by expanding the right-hand sides in the limit $g \rightarrow 1$, $L \rightarrow \infty$, $k \rightarrow 0$ at fixed w and kL . As expected, as long as $\zeta \neq 0$, we obtain a result that is independent of ζ : the FSS behavior only depends on the nature of the boundary conditions, but not on the specific values of the boundary fields.

A localized state exists only for $w \geq 1$. If we set $h = \delta/L$, the parameter δ is a solution of the equation

$$\delta = w \tanh \delta. \quad (46)$$

The corresponding excitation energy is

$$\mathcal{E}_{\text{loc}} = \frac{2}{L} \sqrt{w^2 - \delta^2}. \quad (47)$$

Note that $\delta \rightarrow 0$ for $w \rightarrow 1$, so that $\mathcal{E}_{\text{loc}}L \rightarrow 2$ in the limit. On the other hand, for $w \rightarrow \infty$ we obtain $\delta \rightarrow w(1 - 2e^{-2w})$ so that $\mathcal{E}_{\text{loc}}L \approx 4we^{-w}$, consistently with Eq. (31).

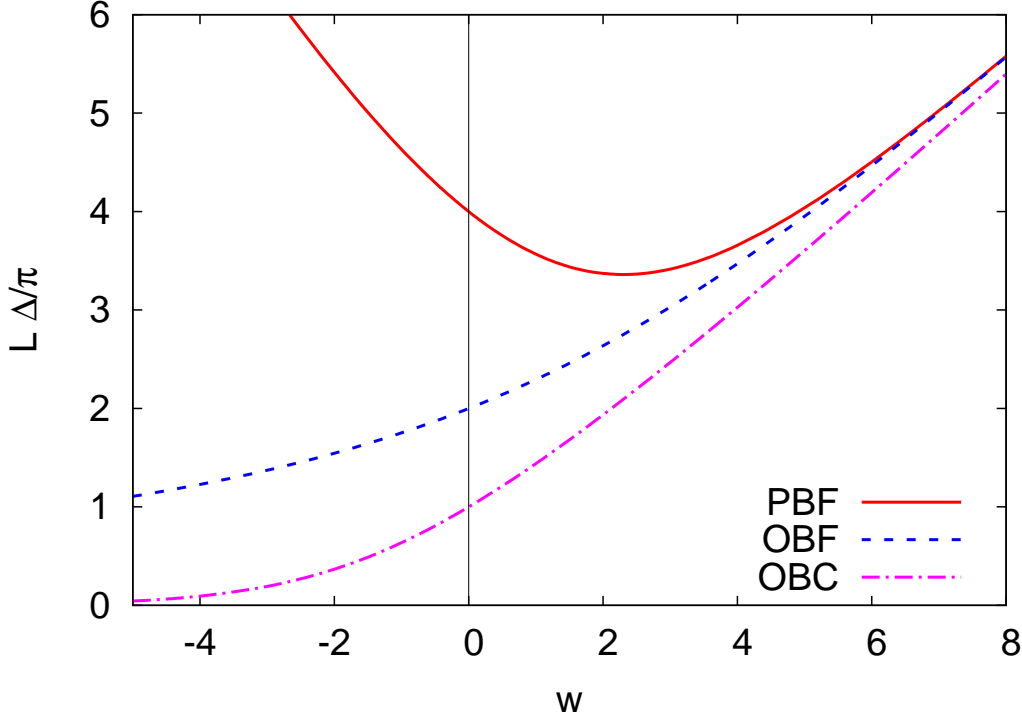


Figure 2. (Color online) FSS curves for $L\Delta/\pi$, for PBF, OBF, and OBC, as a function of w . For $w = 0$, $L\Delta/\pi = 4, 2, 1$ in the three cases, respectively.

The propagating modes can be written as $k = \epsilon_n/L$, where ϵ_n are the positive solutions of the equation

$$\epsilon_n = w \tan \epsilon_n, \quad (48)$$

with $(n - 3/2)\pi \leq \epsilon_n \leq (n - 1/2)\pi$ (the solution with $n = 1$ only exists for $0 < w \leq 1$). The corresponding excitation energies are then $\mathcal{E}_n = 2\sqrt{w^2 + \epsilon_n^2}$. Using these results we obtain for the energy gap in the FSS limit:

$$\begin{aligned} L\Delta(w) &= 2\sqrt{w^2 + \epsilon_3^2} \pm 2\sqrt{w^2 + \epsilon_2^2} & \text{for } w \leq 0, \\ L\Delta(w) &= 2\sqrt{w^2 + \epsilon_2^2} \pm 2\sqrt{w^2 + \epsilon_1^2} & \text{for } 0 < w \leq 1, \\ L\Delta(w) &= 2\sqrt{w^2 + \epsilon_2^2} \pm 2\sqrt{w^2 - \delta^2} & \text{for } w > 1. \end{aligned} \quad (49)$$

The two signs refer to the case of parallel (plus sign) and opposite (minus sign) boundary fields. The curves are reported in Fig. 2 together with the corresponding OBC scaling function. In the paramagnetic phase all curve have a similar shape — they coincide asymptotically — while in the phase $g < 1$ ($w < 0$), the behavior is clearly different. For $w \rightarrow -\infty$, we have $L\Delta_{\text{PBF}}(w) \sim 4|w|$, $L\Delta_{\text{OBF}}(w) \sim 3\pi^2/|w|$, and $L\Delta_{\text{OBC}}(w) \sim 4|w|e^w$.

It is interesting to discuss the scaling corrections, that can be easily shown to decay as $1/L$, as it occurs for $\zeta = 0$. In Ref. [21] we argued that such corrections are not associated with irrelevant boundary operators, which give rise to corrections of order L^{-2} , but that they should be interpreted as due to nonlinear scaling fields. The same

holds for $\zeta \neq 0$. First, one should consider the effective length L_{eff} defined in Eq. (42). Then, one should consider the nonlinear scaling field u_μ associated with $g - 1$ and, finally, rescale the energies with the *sound velocity* $c(g)$. The nonlinear scaling fields do not depend on the boundary conditions, hence we can use the expressions reported in Ref. [21]:

$$c(g) = 2\sqrt{g} \quad u_\mu = (g - 1)/\sqrt{g}. \quad (50)$$

Then, we define the new scaling variable

$$\tilde{w} = u_\mu L_{\text{eff}} \quad (51)$$

and express ϵ_n and δ as functions of \tilde{w} . A somewhat lengthy calculation shows that $c(g)L\Delta/2$ can be written as in Eq. (49), with \tilde{w} replacing w , with corrections that scale as L_{eff}^{-2} . As expected, the leading corrections cancel out.

6. The magnetized phase

Let us now consider the case $g < 1$. In the infinite-volume limit, there exist two degenerate ground states $|+\rangle$ and $|-\rangle$, which differ by the value of the magnetization [5]

$$m_\pm = \lim_{h \rightarrow 0^\pm} \lim_{L \rightarrow \infty} \langle \sigma_i^{(1)} \rangle = \pm m_0, \quad m_0 = (1 - g^2)^{1/8}, \quad (52)$$

where h is a bulk magnetic field applied along the x direction. For a chain of finite size L , the degeneracy is lifted. In the OBC case, the energy difference between the two lowest-energy states vanishes exponentially as L increases [5]:

$$\Delta_{\text{OBC}} \equiv E_1 - E_0 = 2(1 - g^2)g^L [1 + O(g^{2L})]. \quad (53)$$

Moreover, $m(x) = 0$ by symmetry, and

$$\frac{G(L/2, x)}{m_0^2} \rightarrow 1 \quad \text{for } L \rightarrow \infty. \quad (54)$$

These are the standard features of a quantum ferromagnetic phase with a spontaneously broken \mathbb{Z}_2 symmetry.

We now extend the discussion to the case in which boundary fields are present, considering equal PBF and OBF. To identify localized states, we consider Eq. (28). The relevant solutions are associated with the poles in the right-hand side of the equation, see Eq. (29). It is immediate to verify that there are no poles for $\zeta^2 > 1 - g$, while a pole exists in the opposite case. Therefore, we distinguish three different cases, depending on whether ζ is smaller, larger, or equal to

$$\zeta_c(g) = (1 - g)^{1/2}. \quad (55)$$

6.1. Spectrum

6.1.1. Low-field regime, $\zeta < \zeta_c(g)$. For $\zeta < \zeta_c(g)$, the two lowest-energy excitations corresponding to \mathcal{E}_1 and \mathcal{E}_2 are localized. We have $k = ih$ ($h > 0$) with

$$e^h = s(1 + \delta), \quad s = \frac{1 - \zeta^2}{g}, \quad (56)$$

where $s > 1$ and δ is a correction term. Let us first obtain a large- L expression for δ that is uniform as $\zeta \rightarrow 0$. This requires particular care as the right-hand side of Eq. (28) has a different singular behavior for $\zeta = 0$ and $\zeta \neq 0$. For $\zeta = 0$, it has a simple pole as $e^h \rightarrow s = 1/g$. On the other hand, for $\zeta \neq 0$, it has a double pole for $e^h \rightarrow s$.

To compute δ we set $e^h = s$ in all terms of Eq. (28) that are not relevant for the singular behavior as $L \rightarrow \infty$, i.e., we write

$$s^{2L} = \frac{(1 - ge^h)}{C_1 g (e^h - s)^2}. \quad (57)$$

with

$$C_1 = \frac{s(s - g)}{g(s^2 - 1)^2}. \quad (58)$$

Equation (57) is a second-order algebraic equation of e^h , whose solutions are

$$e^h = s + \frac{s^{-2L}}{2C_1 g} \left(\pm \sqrt{4C_1 g \zeta^2 s^{2L} + g^2} - g \right). \quad (59)$$

The energies $\mathcal{E}^2/4 = 1 + g^2 - 2g \cosh h$ are correspondingly

$$\frac{1}{4} \mathcal{E}_{\pm}^2 = \frac{\zeta^2(1 - g^2 - \zeta^2)}{(1 - \zeta^2)} - \frac{g(1 - s^2)^3 s^{-2L}}{2(g - s)s^3} \left(\pm \sqrt{4C_1 g \zeta^2 s^{2L} + g^2} - g \right) \quad (60)$$

and $\mathcal{E}_1 = \mathcal{E}_+$, $\mathcal{E}_2 = \mathcal{E}_-$.

There are now two interesting cases. First, we take the limit $L \rightarrow \infty$ at fixed $\zeta \neq 0$. We can then simplify Eq. (60), obtaining

$$\frac{1}{4} \mathcal{E}_{\pm}^2 = \frac{\zeta^2(1 - g^2 - \zeta^2)}{(1 - \zeta^2)} \pm \zeta \frac{g(1 - s^2)^3 s^{-L}}{(s - g)s^3} \sqrt{C_1 g}. \quad (61)$$

These results imply

$$\Delta_{\text{PBF}} \equiv \mathcal{E}_2 + \mathcal{E}_1 = 4\zeta \sqrt{\frac{1 - g^2 - \zeta^2}{1 - \zeta^2}} + O(s^{-L}), \quad (62)$$

$$\Delta_{\text{OBF}} \equiv \mathcal{E}_2 - \mathcal{E}_1 = \frac{2g(s^2 - 1)^2}{(s - g)s^2} s^{-L} + O(s^{-2L}). \quad (63)$$

In the PBF case the gap is finite and proportional to ζ for small fields. Instead, Δ_{OBF} vanishes exponentially, as in the OBC case (which corresponds to vanishing boundary fields).

A second possibility consists in considering the FSS limit around $\zeta = 0$. As discussed in Ref. [22], the ratio $\Delta_{\text{PBF}}(\zeta)/\Delta_{\text{OBC}}$ is expected to become a function of $\kappa = \zeta/\Delta_{\text{OBC}}$ (to compare with the formulae of Ref. [22] note that the energy associated with the perturbation is here proportional to ζ , without additional factors of L). In this limit $s^L\zeta \approx g^L\zeta$ is proportional to κ . Using the expression for Δ_{OBC} reported in Eq. (53), we obtain

$$\frac{\mathcal{E}_{\pm}}{\Delta_{\text{OBC}}} = \frac{1}{2}\sqrt{1 + 16(1 - g^2)\kappa^2} \mp \frac{1}{2}, \quad (64)$$

so that

$$\frac{\Delta_{\text{PBF}}(\zeta)}{\Delta_{\text{OBC}}} = \sqrt{1 + 16(1 - g^2)\kappa^2}. \quad (65)$$

Note that the scaling function agrees with that predicted in Ref. [22]. We can also consider the ratio $\Delta_{\text{OBF}}(\zeta)/\Delta_{\text{OBC}}$ in the same limit, but in this case we obtain that the ratio is simply equal to 1, i.e., independent of κ . The reason can be easily understood. For OBF the energy associated with the perturbation is zero—the contributions of the two boundaries cancel—hence $\kappa = 0$ identically.

6.1.2. Large-field phase, $\zeta > \zeta_c(g)$. For $\zeta > \zeta_c(g)$ there are no localized states. The secular equation (27) can be rewritten as

$$\tan kL = \sin kf(k, \zeta, g), \quad f(0, \zeta, g) \neq 0. \quad (66)$$

For $L \rightarrow \infty$, the solutions can be parametrized as

$$k_n = \frac{\pi n}{L} + \frac{a_n}{L^2}. \quad (67)$$

It follows that

$$\tan \frac{a_n}{L} \approx \sin \left(\frac{\pi n}{L} + \frac{a_n}{L^2} \right) f(k_n, \zeta, g). \quad (68)$$

For large values of L we obtain finally

$$a_n = an = \pi n f(0, \zeta, g) = \pi n \frac{g(1 - g + \zeta^2)}{(1 - g)(1 - g - \zeta^2)}. \quad (69)$$

Note that the correction term a_n diverges as $\zeta \rightarrow \zeta_c(g)$ and has a finite limit as $\zeta \rightarrow \infty$. Moreover, the explicit form of the Hamiltonian is only relevant for the corrections. It follows

$$\mathcal{E}_n = 2(1 - g) + \frac{g}{1 - g} \frac{\pi^2 n^2}{L^2} + \frac{2ag}{1 - g} \frac{\pi n^2}{L^3} + O(L^{-4}). \quad (70)$$

We obtain finally

$$\Delta_{\text{PBF}} = 4(1 - g) + \frac{5g}{1 - g} \frac{\pi^2}{L^2} + O(L^{-3}), \quad (71)$$

$$\Delta_{\text{OBF}} = \frac{3g}{1 - g} \frac{\pi^2}{L^2} + \frac{6g^2(1 - g + \zeta^2)\pi^2}{(1 - g)^2(1 - g - \zeta^2)L^3} + O(L^{-4}). \quad (72)$$

For OBF, the gap vanishes for $L \rightarrow \infty$. However, while the approach is exponential for $\zeta < \zeta_c(g)$, we have $\Delta_{\text{OBF}} \sim L^{-2}$ for large fields. For PBF, the system is gapped as for $\zeta < \zeta_c$. However, in this case corrections are of order L^{-2} .

6.1.3. *Intermediate state*, $\zeta = \zeta_c(g)$. The gap equation is particularly simple. We obtain a solution $\cos k = 1$ and

$$\frac{\sin(L+1)k}{\sin Lk} = g. \quad (73)$$

Hence $\mathcal{E}_1 = 2(1-g)$ with no L dependence. As for the other states we obtain

$$\mathcal{E}_{m+1} = 2(1-g) + \frac{gm^2\pi^2}{1-g} \frac{1}{L^2} - \frac{2gm^2\pi^2}{(1-g)^2} \frac{1}{L^3}, \quad (74)$$

with $m = 1, \dots, L$. It follows $\Delta_{\text{PBF}} = 4(1-g) + O(L^{-2})$, as for $\zeta > \zeta_c$. However, corrections, of order L^{-2} , are a factor of five smaller compared to the large-field case. For OBF we obtain the asymptotic behavior

$$\Delta_{\text{OBF}} = \frac{g}{1-g} \frac{\pi^2}{L^2} - \frac{2g\pi^2}{(1-g)^2 L^3} + O(L^{-4}). \quad (75)$$

As in the large-field case, Δ_{OBF} scales as L^{-2} . However, the prefactor differs by a factor of 3 from that obtained for $\zeta > \zeta_c$, cf. Eq. (72).

6.2. Magnetization and correlation function

We wish now to compute the ground-state magnetization and the corresponding two-point spin-spin correlation function in the magnetized phase, i.e., for $g < 1$. In the PBF case, the system is magnetized, hence we expect $m(i)$ and $G(i, j)$ to be both independent of i and j , except possibly close to the boundaries, and to be equal to m_0 and m_0^2 , respectively, where m_0 is given in Eq. (52). Thus, the boundary magnetic fields have the only role of lifting the degeneracy.

The OBF case is more interesting. In Appendix B we have fully characterized the ground state of the model for small values of g . We find that for it is ferromagnetic for $\zeta < \zeta_c$ (this is consistent with the results for the gap discussed above). For $\zeta > \zeta_c$ kink states [1] are the relevant low-energy excitations, while for $\zeta = \zeta_c$ the ground state is a superposition of kink and ferromagnetic states. The exact knowledge of the ground state allows us to compute the ground-state magnetization and the correlation function perturbatively in g . For OBF we find that $m(i) = \langle \sigma_i^{(1)} \rangle$ vanishes in the low-field case except at the boundaries, depends linearly on i for $\zeta = \zeta_c(g)$, and varies in a simple fashion for $\zeta > \zeta_c(g)$. We expect the same space dependence for all finite values of $g < 1$ in the large- L universal limit, modulo a multiplicative renormalization. If we set $x = i - L/2$ and $\ell = L/2$, so that the center of the chain corresponds to $x = 0$, we predict

$$\begin{aligned} \frac{m(x)}{m_0} &= \frac{x}{\ell} + \frac{1}{\pi} \sin \frac{\pi x}{\ell} & \zeta > \zeta_c, \\ \frac{m(x)}{m_0} &= \frac{x}{\ell} & \zeta = \zeta_c, \\ \frac{m(x)}{m_0} &= 0 & \zeta < \zeta_c. \end{aligned} \quad (76)$$

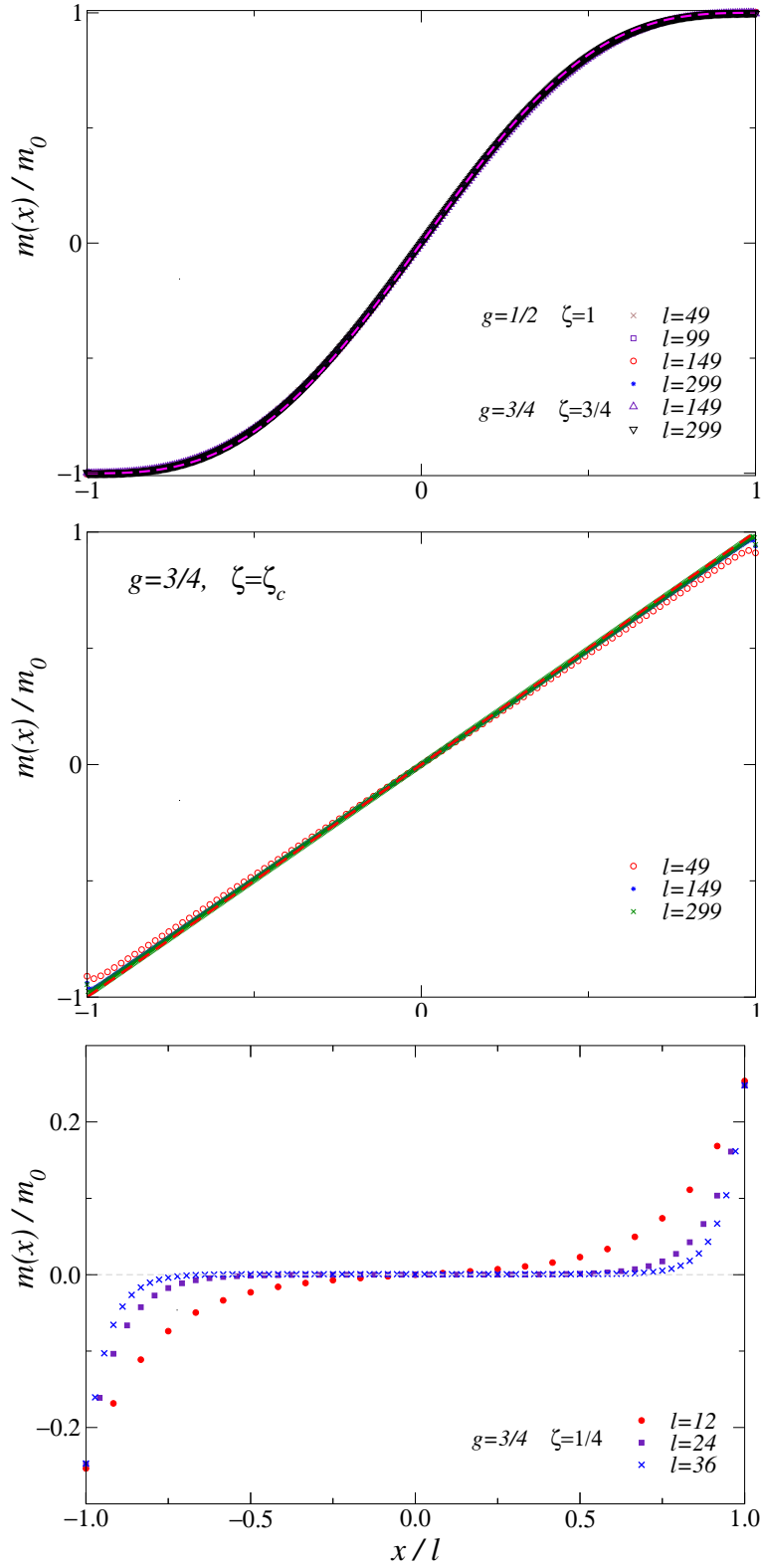


Figure 3. Plots of $m(x)/m_0$ versus x/l for OBF in the ferromagnetic phase $g < 1$. Here $L = 2\ell + 1$, $x = 0$ at the center of the chain. Top: Results for $g = 1/2$, $\zeta = 1$ and $g = 3/4$, $\zeta = 3/4$ (large-field kink phase). Middle: Results for $g = 3/4$ at $\zeta = \zeta_c = \sqrt{1-g}$. Bottom: Results for $g = 3/4$ and $\zeta = 1/4$ (small-field magnetized phase). The dashed lines barely visible on top of the data correspond to the theoretical curves (76).

These relation should hold in the limit $x \rightarrow \infty$, $\ell \rightarrow \infty$ at fixed x/ℓ , except possibly at the boundary, i.e., for $x/\ell = \pm 1$. Here m_0 is the bulk magnetization of the system in the infinite-volume limit defined in Eq. (52). It is interesting to note that the linear behavior of the magnetization for $\zeta = \zeta_c$ is due to the fact that the ground state is translationally invariant: the space probability of the kinks is independent of x . Due to the presence of the boundary fields, the translation invariance of the kink space distribution is not trivial and, indeed, it does not hold for $\zeta > \zeta_c$.

To check these predictions and study the approach to the asymptotic behavior, we perform numerical simulations using the density matrix renormalization-group (DMRG) method [30]. For convenience, we consider chains with odd L , setting $L = 2\ell + 1$ (since we are considering ferromagnetic interactions, the low-energy properties do not depend on this feature, unlike the antiferromagnetic case, see, e.g., Ref. [31]). The results for the magnetization are shown in Fig. 3. For $\zeta < \zeta_c$, the magnetization vanishes in a large interval around $x = 0$, assuming positive and negative values only close to the boundaries. Note that the region in which $m(x) \neq 0$ shrinks as L increases, confirming the validity of Eq. (76) in the large- L limit at fixed x/ℓ . For $\zeta > \zeta_c$ we show results for two values of g . Once we renormalize $m(x)$ by using m_0 , i.e., we consider the ratio $m(x)/m_0$, results fall one on top of the other, confirming universality. The results are in full agreement with the expressions (76).

The same arguments apply to the correlation function $G(i, j)$. Extending the small- g results of Appendix B to the whole low- g phase, we predict

$$\frac{G(i, j)}{m_0^2} = 1 - \frac{1}{m_0} |m(i) - m(j)| \quad (77)$$

in the large- L limit. Therefore, the correlation function should be constant in the magnetized phase, $G(i, j) = m_0^2$, it should depend linearly on $|i - j|$ for $\zeta = \zeta_c$, while it should have a sinusoidal dependence in the kink phase. Again, we check these predictions by comparing them with DMRG data. They are reported in Fig. 4. The DMRG data approach the theoretical predictions with increasing L , confirming the theoretical predictions.

7. Magnet-to-kink transition for $g < 1$

As already discussed in Ref. [23], in the case of OBF and for $g < 1$, an interesting universal scaling behavior is observed for $\zeta \rightarrow \zeta_c(g)$. Such a transition is uniquely characterized by the nature of two phases occurring for $\zeta < \zeta_c$ and $\zeta > \zeta_c$: on one side the ground state is ferromagnetic, while on the other side kink states are the relevant low-energy excitations. This characterization is confirmed by the analysis of the Ising chain on a ring with a bond defect: at the boundary of the two phases one observes [23] a behavior analogous to the one discussed here. Here, we will report the computation of the energy gap—the result was already presented in Ref. [23]—and additional results for the local magnetization, correlation function, and entanglement entropy. Moreover,

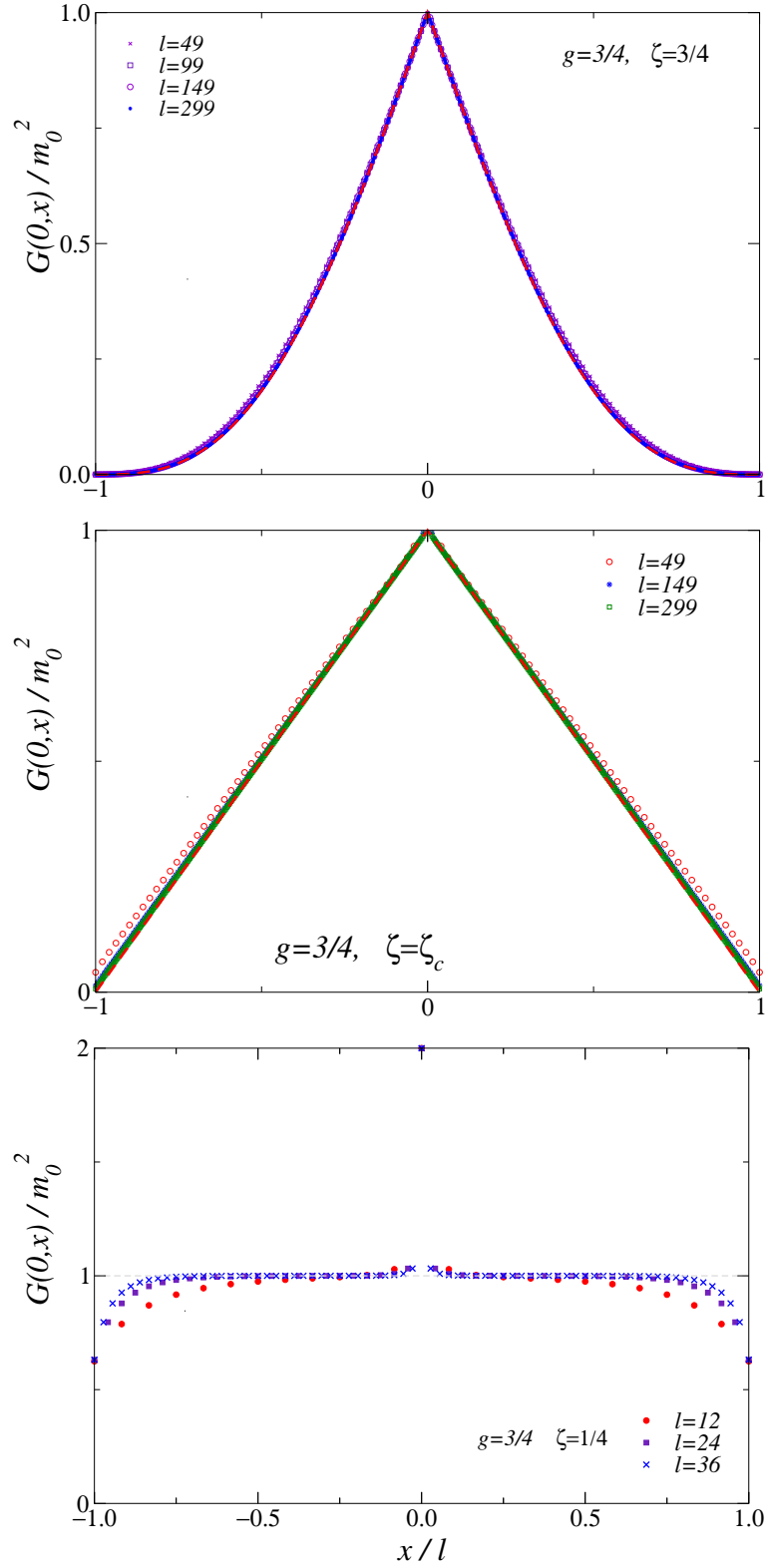


Figure 4. Plots of $G(y = 0, x)/m_0$ versus x/ℓ for OBFF ($L = 2\ell + 1$, $x = y = 0$ at the center of the domain). Top: Results for $g = 3/4$, $\zeta = 3/4$ (large-field kink phase). Middle: Results for $g = 3/4$ at $\zeta = \zeta_c = \sqrt{1-g}$. Bottom: Results for $g = 3/4$ and $\zeta = 1/4$ (small-field magnetized phase). The dashed lines barely visible on top of the data correspond to the theoretical curves obtained by using Eqs. (76) and (77).

we will discuss the density of the fermionic modes in the equivalent fermionic picture of the model [28, 29], showing that the transition can be interpreted as a localization transition of the fermionic states at the boundaries.

The crossover behavior around the transition is parametrized in terms of the scaling variable [23]

$$\zeta_s = \frac{\sqrt{1-g}}{g} L (\zeta - \zeta_c). \quad (78)$$

Then, in the large- L limit we have

$$\Delta_{\text{OBF}}(\zeta) \approx \Delta_{\text{OBF}}(\zeta_c) f_\Delta(\zeta_s), \quad \xi/L \approx f_\xi(\zeta_s). \quad (79)$$

In general, the scaling functions $f_\Delta(\zeta_s)$ and $f_\xi(\zeta_s)$ are expected to be universal modulo a g -dependent normalization (which is independent of the observable considered) of the argument ζ_s . The g dependent prefactor appearing in Eq. (78) is the required nonuniversal factor. It is determined in Sec. 7.1, analyzing the scaling behavior of the gap Δ_{OBF} . According to renormalization-group theory, this normalization factor is independent of the observable considered, hence also the scaling functions of other observables should be independent of g apart from a multiplicative factor (not present if renormalization-group invariant ratios are considered), once ζ_s is used as scaling variable. The results we will present for the magnetization and the two-point correlation function confirm this prediction.

Beside the gap $\Delta_{\text{OBF}}(\zeta)$, we also consider the integrated correlation χ defined in Eq. (8). It satisfies the scaling relation

$$\chi = m_0^2 L f_\chi(\zeta_s), \quad (80)$$

where $f_\chi(\zeta_s)$ is universal, i.e., g independent. These results allow us to define the RG dimensions of the different operators. In general, we expect

$$\Delta_{\text{OBF}}(\zeta) = L^{-z} f_\Delta[L^{y_\zeta}(\zeta - \zeta_c)], \quad \chi = A_\chi L^{d-y_\sigma} f_\chi[L^{y_\zeta}(\zeta - \zeta_c)]. \quad (81)$$

Comparison with our results allows us to identify $z = 2$, $y_\zeta = 1$, and $y_\sigma = 0$. The latter result is consistent with the fact that a bulk magnetic field coupled to $\sigma^{(1)}$ drives a first-order quantum transition, see, e.g., Ref. [22].

By defining ζ_s as in Eq. (78) we have implicitly assumed that we are fixing g and varying ζ close to the critical value $\zeta_c(g)$. In some contexts, however, it is more natural to consider a different point of view. The boundary field strength ζ is fixed (it should satisfy $\zeta < 1$) and g is varied in a neighborhood of the critical value $g_c = 1 - \zeta^2$. In this case we have

$$\zeta_s = \frac{1}{2(1 - \zeta^2)} (g - g_c) L, \quad (82)$$

where the ζ dependent prefactor guarantees that scaling functions are the same for all values of ζ .

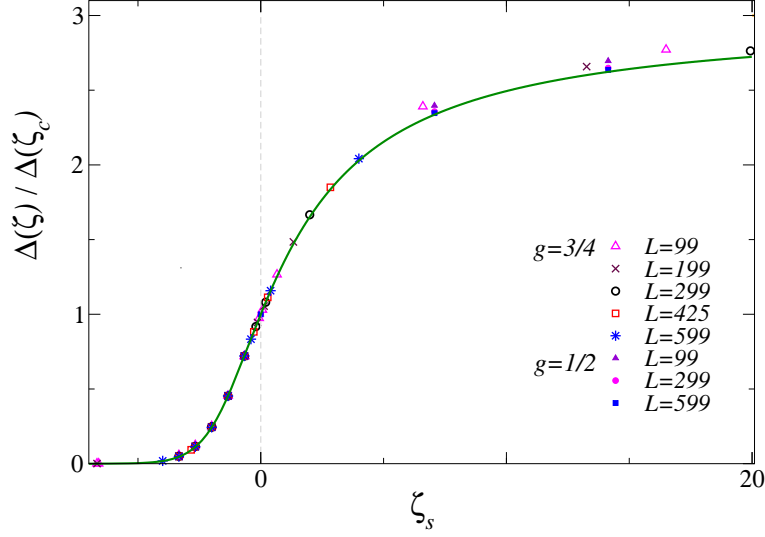


Figure 5. (Color online) Scaling behavior of the gap Δ_{OBF} around $\zeta = \zeta_c$. The DMRG estimates (points) of $\Delta_{\text{OBF}}(\zeta)/\Delta_{\text{OBF}}(\zeta_c)$ approach the universal theoretical curve for $L \rightarrow \infty$ (full line).

7.1. Scaling function for the energy gap

To determine the scaling behavior of the energy gap $\Delta_{\text{OBF}}(\zeta)$, we first simplify the secular equation (25), by taking the limit $\zeta \rightarrow \zeta_c$ at fixed ζ_s . In this limit k scales as $1/L$, so that we set $k = z/L$. For $L \rightarrow \infty$ the secular equation becomes

$$4\zeta_s z + (4\zeta_s^2 - z^2) \tan z = 0. \quad (83)$$

Expressing $\tan z$ as a function of $\tan z/2$, we find that the solutions of Eq. (83) satisfy one of the two equations

$$\tan \frac{z}{2} = -\frac{z}{2\zeta_s}, \quad (84)$$

$$\tan \frac{z}{2} = \frac{2\zeta_s}{z}. \quad (85)$$

If $z_{a1} < z_{a2} < \dots$ and $z_{b1} < z_{b2} < z_{b3} \dots$ are the positive solutions of Eqs. (84) and (85), respectively, it is easy to verify that $z_{b1} < z_{a1} < z_{b2} < \dots$ for $\zeta_s \geq 0$ and $\zeta_s \leq -1$. For $-1 \leq \zeta_s < 0$ we have instead $z_{a1} < z_{b1} < z_{a2} \dots$. For $\zeta_s < 0$ there are also localized solutions with $k = iu/L$. The parameter u satisfies one of the two equations

$$\tanh \frac{u}{2} = -\frac{u}{2\zeta_s}, \quad (86)$$

$$\tanh \frac{u}{2} = -\frac{2\zeta_s}{u}. \quad (87)$$

Eq. (87) has a positive solution u_b for $\zeta_s < 0$, while Eq. (86) has a positive solution u_a satisfying $u_a < u_b$ only for $\zeta_s < -1$. These results allow us to determine the scaling function defined in Eq. (79). We obtain $f_\Delta(\zeta_s) = (z_{a1}^2 - z_{b1}^2)/\pi^2$ for $\zeta_s > 0$, $f_\Delta(\zeta_s) = (z_{a1}^2 + u_b^2)/\pi^2$ for $-1 < \zeta_s < 0$ and $f_\Delta(\zeta_s) = (u_b^2 - u_a^2)/\pi^2$ for $\zeta_s < -1$.

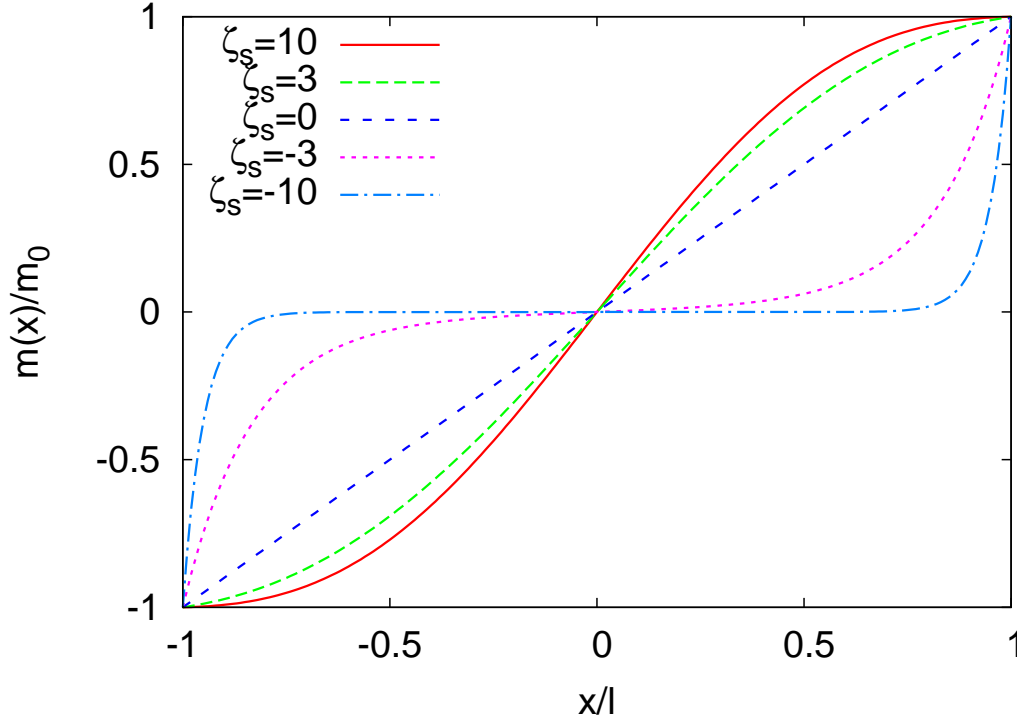


Figure 6. (Color online) Rescaled local magnetization $m(x)/m_0$ versus x/ℓ for $\zeta_s = -10, -3, 0, 3, 10$.

We can easily determine the asymptotic behaviors. For small ζ_s we have

$$f_{\Delta}(\zeta_s) = 1 + \frac{4\zeta_s}{\pi^2} + O(\zeta_s^2), \quad (88)$$

while for $\zeta_s \rightarrow \infty$ we have

$$f_{\Delta}(\zeta_s) = 3 - \frac{6}{\zeta_s} + O(\zeta_s^{-2}). \quad (89)$$

Finally, for $\zeta_s \rightarrow -\infty$ we have

$$f_{\Delta}(\zeta_s) \approx \frac{32}{\pi^2} \zeta_s^2 e^{2\zeta_s}. \quad (90)$$

The theoretical curve is shown in Fig. 5. The DMRG data confirm the theoretical calculation: the numerical estimates of the ratio $\Delta_{\text{OBF}}(\zeta)/\Delta_{\text{OBF}}(\zeta_c)$ clearly approach the scaling curve $f_{\Delta}(\zeta_s)$ with increasing L .

7.2. Magnetization and two-point function

Let us now consider the behavior of the correlations close to ζ_c . The local magnetization $m(i)$ and the correlation function $G(i, j)$ are computed exactly in the limit $g \rightarrow 0$ in Appendix B.4. As we have already done in Sec. 6.2, we extend these expressions to all

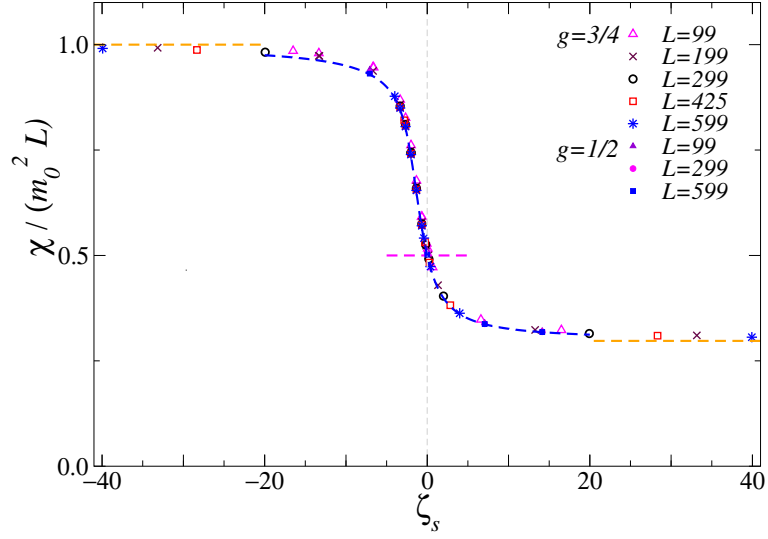


Figure 7. (Color online) Crossover scaling curve for $\chi/(m_0^2 L)$ versus ζ_s . We report the theoretical prediction (dashed line) and DMRG data for $g = 1/2$ and $g = 3/4$ to confirm universality. Note the limiting values: $f_\chi(0) = 1/2$, $f_\chi(-\infty) = 1$, and $f_\chi(\infty) \approx 0.297$, indicated by the horizontal dashed lines.

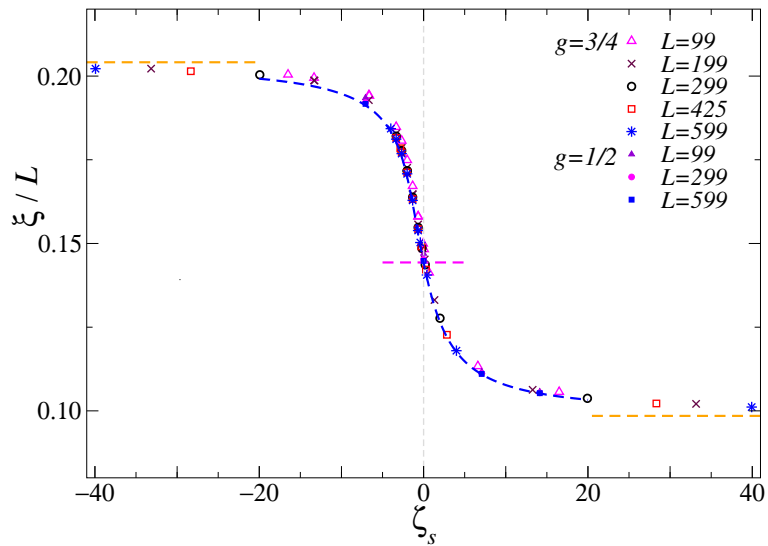


Figure 8. (Color online) Crossover scaling curve $\xi/L = f_\xi(\zeta_s)$ for the correlation length ξ . We report the theoretical prediction for the asymptotic scaling behavior and DMRG data for $g = 1/2$ and $g = 3/4$ to confirm universality. Note the limiting values: $f_\xi(0) = 1/\sqrt{48}$, $f_\xi(-\infty) = 1/\sqrt{24}$, and $f_\xi(\infty) \approx 0.0985$.

values of g satisfying $g < 1$, by replacing $m(i)$ with $m(i)/m_0$ and $G(i, j)$ with $G(i, j)/m_0^2$. Therefore, we predict for $\zeta_s > 0$

$$\frac{m(x)}{m_0} = \frac{z}{z + \sin z} \left[\frac{1}{z} \sin \left(\frac{zx}{\ell} \right) + \frac{x}{\ell} \right], \quad (91)$$

where z is the smallest positive solution ($z = z_{b1}$) of Eq. (85), $x = i - L/2$, and $\ell = L/2$, as before. For $\zeta_s < 0$ we have instead

$$\frac{m(x)}{m_0} = \frac{u}{u + \sinh u} \left[\frac{1}{u} \sinh \left(\frac{ux}{\ell} \right) + \frac{x}{\ell} \right], \quad (92)$$

where u is the solution ($u = u_b$) of Eq. (87). As for the correlation function $G(i, j)$ it satisfies Eq. (77). It is important to stress that the previous expressions, although derived for small values of g , are expected to be *exact* for any $g < 1$. For instance, since $m(x)/m_0$ is a dimensionless renormalization-group invariant ratio, it should scale as

$$m(x, \zeta, g, L) = m_0 f_m[a(g)(\zeta - \zeta_c)L, x/L], \quad (93)$$

where f_m is a universal, hence g independent, function. The specific features of the model enter in this expression only through the normalization nonuniversal factor $a(g)$ and the critical value $\zeta_c(g)$. The factor $a(g)$ does not depend on the observable, hence it can be determined by using any quantity. We use the gap Δ_{OBF} , for which we are able to obtain exact results for any $g < 1$, defining $\zeta_s = a(g)(\zeta - \zeta_c)L$. Therefore, f_m as a function of ζ_s and x/L is g independent. Therefore, our results, obtained in the limit $g \rightarrow 0$, hold for any value of g satisfying $g < 1$.

The previous expressions for $m(x)$ hold in the limit $x \rightarrow \infty$, $L \rightarrow \infty$ at fixed x/ℓ and smoothly interpolate between the expressions valid in the different phases. Note that we have $m(i) \rightarrow \pm m_0$ for $x/\ell \rightarrow \pm 1$ in all cases. This result does not however necessarily apply to the boundary points, i.e., for $x/\ell = \pm 1$, as the magnetization is not continuous at the boundary. For instance, in the magnetized phase, $m_i = 0$ in all interior points, while m_1 and $m_L = -m_1$ are nonuniversal functions of the field strength ζ .

A graph of $m(x)/m_0$ for several values of ζ_s as a function of x/ℓ is reported in Fig. 6. As expected, for $\zeta_s \rightarrow -\infty$ the magnetization approaches zero exponentially in an interval that is centered in the middle of the chain and that widens as $|\zeta_s|$ increases. More precisely, for $\zeta_s \rightarrow -\infty$ we have $u \approx -2\zeta_s$ and

$$m(x) = \frac{\sinh 2\zeta_s x/\ell}{\sinh 2\zeta_s}, \quad (94)$$

which shows that $m(x)$ vanishes except in two tiny intervals close to the boundaries of width $\ell/(2|\zeta_s|)$.

To verify the prediction (77) for $G(i, j)$ we compute the scaling functions associated with χ and ξ . They are reported in Appendix B.4 and compared with DMRG data in Figs. 7 and 8. Results with different values of g fall on top of the theoretical curve when plotted versus ζ_s . This confirms our predictions for $G(i, j)$ and the magnetization, as well as the correctness of the nonuniversal prefactor appearing in the definition of ζ_s .

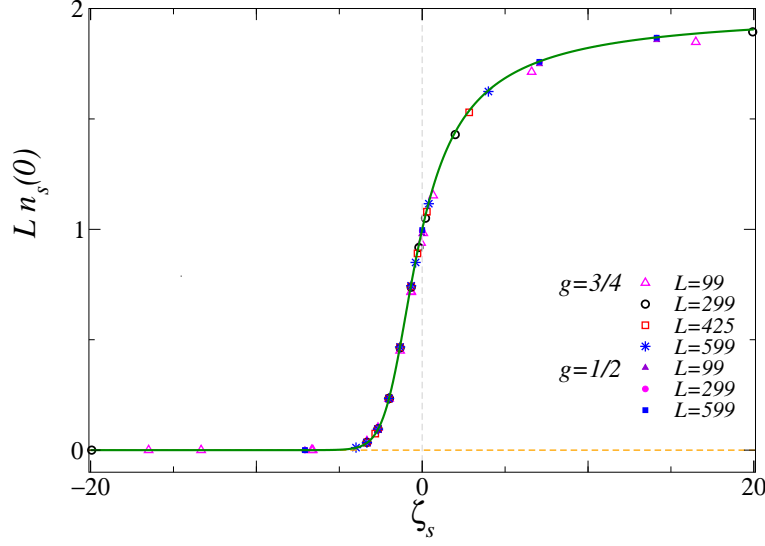


Figure 9. (Color online) Scaling of the subtracted fermionic density at the center of the chain. We plot DMRG data of $Ln_s(0)$ for $g = 3/4$ and $g = 1/2$ versus ζ_s . The full line corresponds the asymptotic analytic curve, cf. Eqs. (98) and (99). Note that $Ln_s(0)$ approaches 2 for $\zeta_s \rightarrow \infty$, 0 for $\zeta_s \rightarrow -\infty$, while it is equal to 1 for $\zeta_s = 0$.

7.3. Equivalent fermionic picture

It is interesting to reinterpret our results in the equivalent fermionic picture of the model. In the ferromagnetic phase, i.e., for $\zeta < \zeta_c$, the lowest eigenstates are superpositions of Majorana fermionic states localized at the boundaries [28, 29]. In finite systems, their overlap does not vanish, giving rise to the splitting $\Delta \sim e^{-L/l_0}$. The coherence length l_0 diverges at the kink-to-magnet transitions as $l_0^{-1} \sim |\ln s| \sim \zeta_c - \zeta$, a behavior analogous to that observed at the order-disorder transition $g \rightarrow 1^-$ where $l_0^{-1} \sim |\ln g|$.

Within this picture, it is natural to consider

$$n(i) = \frac{1 + \langle \sigma_i^{(3)} \rangle}{2}, \quad (95)$$

which can be interpreted as the particle density in the fermionic representation of the Ising chain, see Eq. (11). Its large- L limit is given by [5]

$$n_h = \frac{1}{2} + \frac{1}{2\pi} \int_0^\pi dk \frac{g + \cos k}{\sqrt{1 + g^2 + 2g \cos k}}. \quad (96)$$

We consider the difference

$$n_s(x) \equiv n(i) - n_h, \quad (97)$$

where $x = i - L/2$, as before. Such a quantity has been computed for small values of g in Appendix B.4. The universality argument we have used for $m(i)$ and $G(i, j)$ can be applied to $n_s(x)$. We therefore predict

$$Ln_s(x) = \frac{z}{z + \sin z} \left(1 + \cos \frac{zx}{\ell} \right) \quad (98)$$

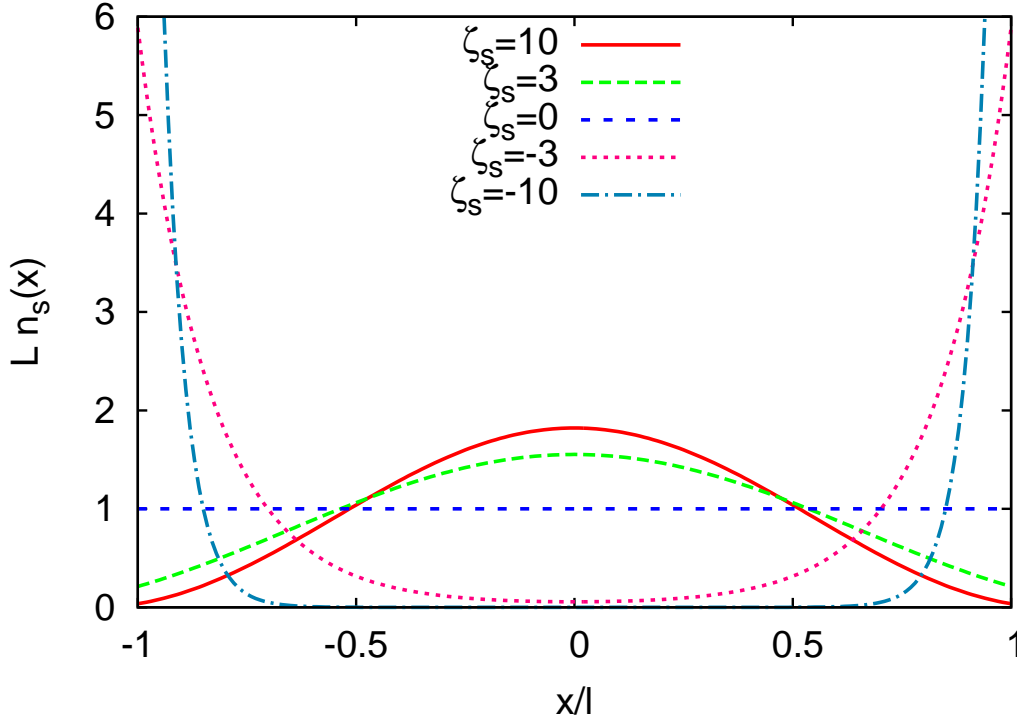


Figure 10. (Color online) Subtracted fermionic density $Ln_s(x)$ versus x/ℓ for $\zeta_s = -10, -3, 0, 3, 10$ ($x = 0$ at the center of the chain).

for $\zeta_s > 0$ and

$$Ln_s(x) = \frac{u}{u + \sinh u} \left(1 + \cosh \frac{ux}{\ell} \right) \quad (99)$$

for $\zeta_s < 0$, where z and u are determined as in the case of the local magnetization. To verify this prediction we compute $n_s(0)$ numerically for $g = 1/2$ and $g = 3/4$. The numerical results are compared with theory in Fig. 9. The agreement confirms the analytic prediction.

The subtracted fermionic density $Ln_s(x)$ is reported in Fig. 10 as a function of x/ℓ . For positive values of ζ_s it has a maximum at the origin and shows that fermions are delocalized. For $\zeta_s = 0$, $Ln_s(0)$ is constant, while for negative values of ζ_s , there is a significant enhancement at the boundary. For $\zeta_s \rightarrow -\infty$, as in the case of the magnetization, $Ln_s(x)$ is different from 0 only close to the boundary, in an interval of width $\ell/2|\zeta_s|$. It is interesting to consider the behavior of $Ln_s(x)$ at the boundaries, i.e., for $x \rightarrow \pm\ell$, which is shown in Fig. 11. In the kink phase, such a quantity scales as $\pi^2/(2\zeta_s^2)$ for $\zeta_s \rightarrow \infty$. On the other hand it diverges as $-2\zeta_s$ for $\zeta_s \rightarrow -\infty$, that is when the magnetized phase is approached. As such, it represents a physically relevant order parameter for the transition, which distinguishes the two different phases.

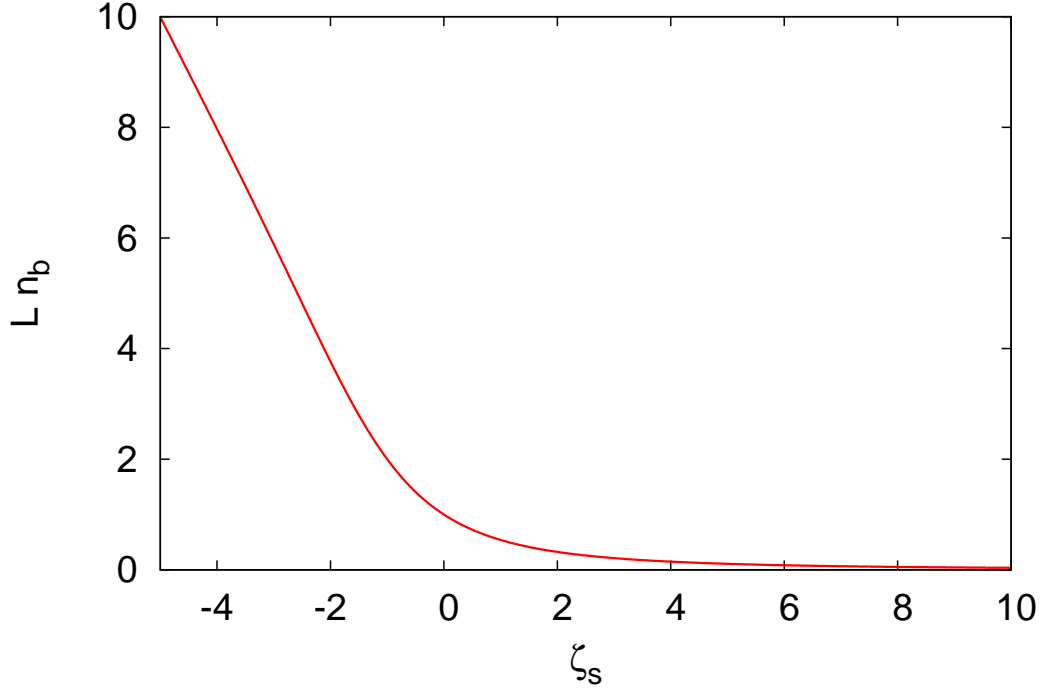


Figure 11. (Color online) Subtracted fermionic density $Ln_b = Ln_s(\pm\ell)$ at the boundaries of the chain versus ζ_s . We have $Ln_b(\zeta_s) \approx \pi^2/(2\zeta_s^2)$ for $\zeta_s \rightarrow \infty$, $Ln_b(\zeta_s) \approx -2\zeta_s$ for $\zeta_s \rightarrow -\infty$, and $Ln_b(0) = 1$.

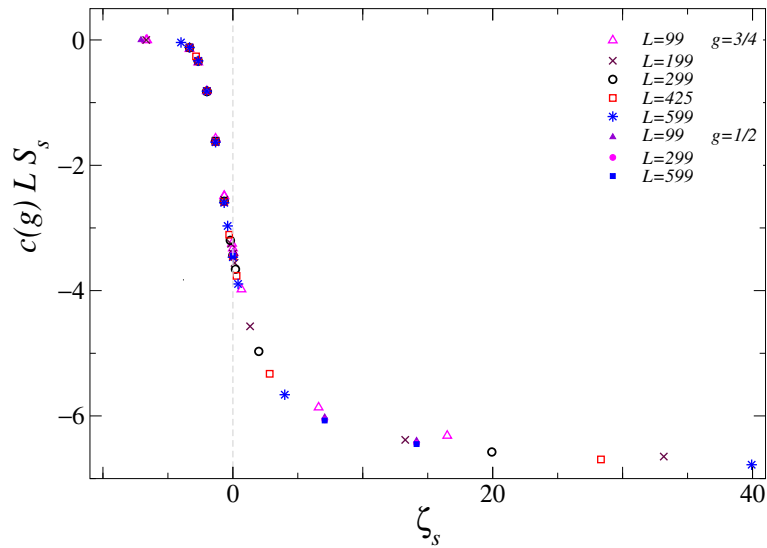


Figure 12. (Color online) Scaling of the subtracted half-chain entanglement entropy. The DMRG data appear to approach an asymptotic scaling curve. The scaling curves for different values of g match after a global nonuniversal rescaling: fixing $c(g = 3/4) = 1$ the optimal matching is obtained for $c(g = 1/2) \approx 1.85$.

7.4. Half-chain entanglement entropy

Finally, we discuss the behavior of the half-chain entanglement entropy [32]. We divide the chain into two connected parts $[-\ell, 0]$ and $[1, \ell]$ and consider the von Neumann entropy

$$S = -\text{Tr} \rho_{[-\ell, 0]} \ln \rho_{[-\ell, 0]}, \quad (100)$$

where $\rho_{[-\ell, 0]}$ is the reduced density matrix of the subsystem $[-\ell, 0]$, i.e.,

$$\rho_{[-\ell, 0]} = \text{Tr}_{[1, \ell]} \rho, \quad (101)$$

and ρ is the density matrix of the ground state. The entanglement entropy S approaches a constant in the large- L limit, except for the critical case $g = 1$ where it increases logarithmically [32]. Its large- L limit for OBC is given by [18]

$$S_{\text{OBC}}(g) = \ln 2 + \frac{1}{12} \left[\ln \frac{g^2}{16\sqrt{1-g^2}} + \left(1 - \frac{g^2}{2}\right) \frac{4I(g)I(\sqrt{1-g^2})}{\pi} \right],$$

$$I(z) = \int_0^1 \frac{dx}{\sqrt{(1-x^2)(1-z^2x^2)}}. \quad (102)$$

In Fig. 12 we plot the difference

$$S_s \equiv S(\zeta, g, L) - S_{\text{OBC}}(g), \quad (103)$$

which shows the scaling behavior

$$S_s \approx L^{-1} f_S(\zeta_s), \quad (104)$$

where f_S is a universal function apart from a multiplicative nonuniversal constant. These results imply that the large- L limit of the half-chain entanglement entropy does not depend on the boundary conditions, being the same for OBC and OBF. However, the $O(L^{-1})$ corrections are affected by the boundary term (2), giving rise to a nontrivial universal behavior around ζ_c .

7.5. Comparison with the existing results for two-dimensional classical models

The results we have obtained allow us to derive exact scaling functions for the classical two-dimensional Ising model in a strip $L \times \infty$ in the presence of two equal magnetic fields on the boundaries. This model has been extensively studied, especially in the case of opposite magnetic fields. In this case, the wetting (or interface localization-delocalization) transition, which is the analog of the magnet-to-kink transition we are considering here, has been extensively studied [33, 34, 35, 36, 37, 38, 39, 40, 41, 42]. We can therefore check some of our results, comparing them with the existing ones in the literature.

The results for the gap Δ_{OBF} obtained in Sec. 7.1 can be used to derive the scaling behavior of the longitudinal correlation length ξ_{\parallel} , defined by $\xi_{\parallel} = 1/\Delta_{\text{OBF}}$. Such a

quantity was computed in the restrictive solid-on-solid model in Ref. [37]. Their result is completely consistent with ours. If our scaling quantities z and u defined in Sec. 7.1 are identified with the quantities $\sqrt{2G_0}$, $\sqrt{2G_1}$ appearing in Ref. [37], we obtain exactly the same expression for ξ_{\parallel}/L^2 .

Several papers study the magnetization profile, which gives information on the behavior of the interface between the two coexisting phases. The behavior in the large-field phase was determined in Ref. [35] by using the restrictive solid-on-solid model. The result is in agreement with our prediction (76) for $\zeta > \zeta_c$. The linear behavior observed at $\zeta = \zeta_c$ was also derived at the wetting transition by using the solid-on-solid model [39]. No exact results are instead available for the magnetization profiles in the whole crossover region, which, in the classical case, is usually parametrized in terms of $[T - T_w(h)]L$, where h is the boundary field and T_w the corresponding wetting temperature (in the quantum-to-classical mapping g corresponds to T , hence this scaling corresponds to varying g at fixed ζ). However, the numerical results for the magnetization reported in Refs. [40, 41, 42] (and, in particular, Fig. 2 of Ref. [40]) appear to be in full agreement with our prediction shown in Fig. 6.

8. Conclusions

We consider the one-dimensional quantum Ising chain in the presence of a transverse magnetic field g [5] and of boundary magnetic fields aligned with the order-parameter spin operator. In particular, we consider fields with equal strength ζ , which have either the same (PBF) or the opposite (OBF) direction, cf. Eqs. (3) and (4). We assume the chain to have length L and derive the finite-size behavior of several quantities in the limit $L \rightarrow \infty$ as a function of ζ .

We derive analytic predictions for the gap in all phases as a function of the boundary field strength. In the paramagnetic quantum phase, the leading behavior is independent of the boundary conditions. At the critical transition $g = 1$, finite-size scaling depends on the boundary fields. The point $\zeta = 0$, corresponding to open boundary conditions, is a surface critical point. We derive analytic expressions for the scaling functions that parametrize the crossover behavior for $g \rightarrow 1$ and any ζ (bulk critical behavior), and for $g = 1$ and $\zeta \rightarrow 0$ (surface critical behavior). In the quantum ferromagnetic phase $g < 1$, if the boundary fields are oppositely aligned, the finite-size behavior drastically changes as ζ varies [23]. For small ζ , the system is in a ferromagnetic phase in which the gap decreases exponentially with the system size. On the other hand, for large fields, kink propagating modes of momenta $1/L$ are the relevant low-energy excitations, so that the gap decreases as $1/L^2$. The two phases are separated by a critical transition at $\zeta = \zeta_c(g)$. Close to this transition, low-energy properties show a universal scaling behavior in terms of the scaling variable $L(\zeta - \zeta_c)$. The transition is only characterized by the nature of the coexisting phases. Indeed, the same transition occurs in Ising rings in the presence of a localized bond defect [23].

It is interesting to interpret our results in the context of two-dimensional classical

Ising models, using the quantum-to-classical mapping. As is well known [1], the quantum Ising chain of length L corresponds to a classical Ising model on a strip of width L , the transverse field playing the role of the temperature. Therefore, our results provide exact predictions for the Ising model in an $L \times \infty$ geometry with boundary fields. Our results for the gap at the critical point can be used to predict the FSS behavior of the longitudinal exponential correlation function $\xi_{\parallel} = 1/\Delta$ as a function of $w = A(T - T_c)L$ and of $\zeta_b = B\zeta L^{1/2}$, where A and B are nonuniversal model-dependent constants. Moreover, our extensive results at the magnet-to-kink transition for $g < 1$ for OBF provide predictions for the finite-size scaling functions at the classical wetting transition (sometimes also called interface localization/delocalization transition [27]) in two dimensions. In particular, we have exact predictions for the FSS behavior of the magnetization profile and of the correlation function of the layer magnetization in the whole crossover region close to the transition.

In the context of the wetting transition, one may also consider a second important surface parameter, which is usually referred to as surface enhancement [34, 24]. While a boundary magnetic field is the most relevant magnetic perturbation that breaks the \mathbb{Z}_2 symmetry at the boundary, surface enhancement is the most relevant (energy-like) perturbation that is \mathbb{Z}_2 invariant. In the context of the quantum chain, such an interaction can be mimicked by adding a term $(h_1\sigma_1^{(3)} + h_L\sigma_L^{(3)})$, localized at the boundary, to the general Ising-chain Hamiltonian. It is not difficult to generalize the results presented here to this more general case (results for the spectrum in the absence of boundary magnetic fields appear in Refs. [8, 12]). At the critical point, this would allow us to study the behavior at the ordinary and extraordinary surface transitions (in the absence of surface enhancement the point $g = 1$, $\zeta = 0$ corresponds to the so-called special transition [34]). Moreover, a complete understanding of the phase behavior for $g < 1$ in the absence of a bulk magnetic field should be possible. In the quantum case, these results would also be relevant for Ising quantum rings with localized site defects, a distinct case with respect to that considered in Ref. [23].

Appendix A. Spectrum determination

Appendix A.1. Preliminary matrix results

In this appendix we collect results on the spectrum of some matrices that are relevant for the discussion. We begin by considering the $n \times n$ matrix (we write it for $n = 5$)

$$A_n(d, b) = \begin{pmatrix} d & b & 0 & 0 & 0 \\ b & d & b & 0 & 0 \\ 0 & b & d & b & 0 \\ 0 & 0 & b & d & b \\ 0 & 0 & 0 & b & d \end{pmatrix}. \quad (\text{A.1})$$

To determine its eigenvalues, we compute

$$a_n(d, b) = \det(A_n(d, b) - \lambda I). \quad (\text{A.2})$$

If we set $\lambda = d - 2b \cos k$, the determinant $a_n(d, b)$ satisfies the recursion relation

$$a_n = 2b \cos k a_{n-1} - b^2 a_{n-2}. \quad (\text{A.3})$$

The solution is

$$a_n b^{-n} = c_1 e^{ikn} + c_2 e^{-ikn}, \quad (\text{A.4})$$

where c_1 and c_2 are arbitrary constant. If we require $a_1 = 2b \cos k$ and $a_2 = b^2(4 \cos^2 k - 1)$, we obtain

$$c_1 = -\frac{ie^{ik}}{2 \sin k}, \quad c_2 = c_1^*. \quad (\text{A.5})$$

It follows

$$a_n = b^n \frac{\sin k(n+1)}{\sin k}. \quad (\text{A.6})$$

The eigenvalues are solutions of the equation $a_n = 0$. We obtain n eigenvalues given by

$$\lambda_m = d - 2b \cos k_m \quad k_m = \frac{\pi m}{n+1}, \quad (\text{A.7})$$

with $m = 1, \dots, n$.

Let us now compute the eigenvectors. Let $(\alpha_1, \dots, \alpha_n)$ be the eigenvector corresponding to eigenvalue λ_m . It satisfies the relations

$$2\alpha_1 \cos k_m + \alpha_2 = 0, \quad (\text{A.8})$$

$$\alpha_{j-1} + 2\alpha_j \cos k_m + \alpha_{j+1} = 0, \quad j = 2, \dots, n-1 \quad (\text{A.9})$$

$$\alpha_{n-1} + 2\alpha_n \cos k_m = 0. \quad (\text{A.10})$$

The solution of the recursion relation (A.9) is

$$\alpha_j = (-1)^j (e_1 e^{ik_m j} + e_2 e^{-ik_m j}), \quad (\text{A.11})$$

where e_1 and e_2 are two arbitrary constants. Requiring $\alpha_2 = -2 \cos k_m \alpha_1$, we obtain $e_1 + e_2 = 0$, so that

$$\alpha_j = (-1)^j e_1 \sin k_m j, \quad (\text{A.12})$$

where we have rescaled e_1 for convenience. Requiring the eigenvector to have unit norm, we obtain

$$\alpha_j = (-1)^j \sqrt{\frac{2}{n+1}} \sin k_m j. \quad (\text{A.13})$$

We also determine the eigenvalues of the matrix

$$\tilde{A}_n(d, b, e) = \begin{pmatrix} e & b & 0 & 0 & 0 \\ b & d & b & 0 & 0 \\ 0 & b & d & b & 0 \\ 0 & 0 & b & d & b \\ 0 & 0 & 0 & b & e \end{pmatrix}, \quad (\text{A.14})$$

which differs from A only for two matrix elements: $\tilde{A}_{n,11}$ and $\tilde{A}_{n,nn}$ are equal to e . Setting again

$$\tilde{a}_n = \det(\tilde{A}_n - \lambda I), \quad (\text{A.15})$$

and $\lambda = d - 2b \cos k$, we obtain

$$\tilde{a}_n = (e - d + 2b \cos k)^2 a_{n-2} - 2b^2(e - d + 2b \cos k) a_{n-3} + b^4 a_{n-4}. \quad (\text{A.16})$$

Using the recursion relation (A.3), we obtain finally

$$\tilde{a}_n = (1 - \delta^2) a_n + 2b\delta(\delta \cos k - 1) a_{n-1}, \quad (\text{A.17})$$

where $\delta = (d - e)/b$.

Appendix A.2. Secular equation

To determine the spectrum of Hamiltonian (9), we compute the eigenvalues of the matrix C defined in Eq. (20). We write them as

$$\lambda = g^2 + 1 - 2g \cos k. \quad (\text{A.18})$$

Note that nothing forbids λ to be larger than $|1 + g|$ or smaller than $|1 - g|$, hence $\cos k$ is not necessarily bounded between -1 and 1 . Hence, we must consider real values of k with $0 \leq k \leq \pi$ and complex values of the form $k = ih$ and $k = \pi + ih$ with $h > 0$.

We are not interested in the zero eigenvalue of C , hence we will only consider the $(L + 1) \times (L + 1)$ matrix formed by the first $(L + 1)$ rows and columns, which we label with the symbol C_{L+1} . Then, we introduce a matrix D_{L+1} defined as (here $L = 4$)

$$D_{L+1} = \begin{pmatrix} g^2 + 1 & g & 0 & 0 & 0 \\ g & g^2 + 1 & g & 0 & 0 \\ 0 & g & g^2 + 1 & g & 0 \\ 0 & 0 & g & g^2 + 1 & g \\ 0 & 0 & 0 & g & g^2 + 1 \end{pmatrix} \quad (\text{A.19})$$

The corresponding secular equations are

$$c_n = \det(C_n - \lambda I) \quad d_n = \det(D_n - \lambda I). \quad (\text{A.20})$$

The determinant d_n has already been computed in Appendix A.1:

$$d_n = g^n \frac{\sin k(n+1)}{\sin k}. \quad (\text{A.21})$$

To determine c_n , we expand the determinant with respect to the first and the last rows. We obtain the following recursion relation:

$$\begin{aligned} c_n &= (g^2 + 1 - J_0^2 - 2g \cos k)(1 - J_L^2 - 2g \cos k) d_{n-2} \\ &\quad + g^2(g^2 + 1 - J_0^2 J_L^2 - 2g \cos k - 2g J_0^2 \cos k) d_{n-3} + g^4 J_0^2 d_{n-4}. \end{aligned} \quad (\text{A.22})$$

A simpler expression is obtained by eliminating d_{n-4} and d_{n-3} , and expressing the result in terms of d_{n-1} and d_{n-2} . This can be done by using the recursion relation satisfied by the determinants d_n , see Eq. (A.3) with $b = g$. We obtain finally

$$c_n = -(1 + g^2 - J_0^2 J_L^2 - 2g \cos k) d_{n-1} + [(1 + g^2)(1 - J_0^2 - J_L^2) + J_0^2 J_L^2 - 2g(1 - J_L^2)(1 - J_0^2) \cos k] d_{n-2}. \quad (\text{A.23})$$

Note that the recursion relation (A.23) is symmetric with respect to the exchange of J_0 and J_L . The eigenvalues of C_n are obtained by requiring $c_n = 0$. Setting $J_0 = J_L = \zeta$ and $n = L + 1$, we obtain Eq. (25). Note that we have simplified $\sin k$ in the denominators, hence Eq. (25) has a spurious solution for $k = 0$. A true solution with $k = 0$ occurs only when the coefficients of d_{n-1} and d_{n-2} in Eq. (A.23) both vanish for $k = 0$. This only occurs when $J_0^2 = J_L^2 = 1 - g$.

Appendix B. Perturbative analysis in the small- g limit for opposite boundary conditions

The low-energy behavior of the model with Hamiltonian (1) can be understood analytically in the limit $g \rightarrow 0$. For $g = 0$, it is trivial to compute the spectrum of Hamiltonian (1) in the presence of the magnetic boundary term (2), since H is diagonal in the basis in which $\sigma_i^{(1)}$ is diagonal. Assuming $\zeta_1 = -\zeta_L = -\zeta$ and $\zeta > 0$, there are two family of states that control the low-energy spectrum. First, we should consider the magnetized states

$$\begin{aligned} |+\rangle &= |1, 1, 1, \dots, 1\rangle, \\ |-\rangle &= |-1, -1, -1, \dots, -1\rangle; \end{aligned} \quad (\text{B.1})$$

then, we should also consider the $(L - 1)$ states (we call them kink states [1])

$$\begin{aligned} |1\rangle_k &= |-1, 1, 1, \dots, 1\rangle, \\ |2\rangle_k &= |-1, -1, 1, \dots, 1\rangle, \\ &\dots \\ |L - 1\rangle_k &= |-1, -1, \dots, -1, 1\rangle. \end{aligned} \quad (\text{B.2})$$

If H_0 is the Hamiltonian for $g = 0$ we have ($J = 1$)

$$H_0|\pm\rangle = -(L - 1)|\pm\rangle, \quad H_0|i\rangle_k = -(L - 3 + 2\zeta)|i\rangle_k. \quad (\text{B.3})$$

The value of ζ determines which of the states is the ground state of the system. For $\zeta < 1$, the ground state is doubly degenerate and spanned by $|+\rangle$ and $|-\rangle$, while for $\zeta > 1$ the $(L - 1)$ kink states are the lowest-energy ones. For $\zeta = 1$, the magnetized and the kink states are degenerate. We wish now to determine how this picture changes when the perturbation

$$H_g = -g \sum_i \sigma_i^{(3)} \quad (\text{B.4})$$

is added.

Appendix B.1. Low-field behavior

Let us first understand the behavior for $\zeta < 1$. For $g = 0$ the ground state is doubly degenerate. Such a degeneracy is lifted by perturbation (B.4). Note, however, that $\langle \pm | H_g^n | \mp \rangle$ vanishes for any $n < L$. Therefore, the energy gap is proportional to g^L , in agreement with the exact results obtained in Sec. 6.

Let us now consider the corrections to the ground state which are proportional to g . At order g , $|+\rangle$ mixes with the states generated by $H_g|+\rangle$, so that we can write

$$\begin{aligned} \psi_+ = & \alpha|+\rangle + \beta|-1, 1, 1, \dots, 1\rangle_1 + \delta|1, 1, \dots, 1, -1\rangle_L + \\ & + \gamma \sum_{i=2}^{L-1} |1, 1, \dots, -1, \dots, 1, 1\rangle_i, \end{aligned} \quad (\text{B.5})$$

where β, γ, δ are of order g and state $|\dots\rangle_i$ is defined so that $\sigma_j|\dots\rangle_i = |\dots\rangle_i$ for $i \neq j$ and $\sigma_i|\dots\rangle_i = -|\dots\rangle_i$. Requiring ψ_+ to be normalized, we immediately obtain $\alpha = 1 + O(g^2)$. The coefficients β, γ , and δ are fixed by the eigenvalue condition

$$H_g|+\rangle = (E_0 - H_0)(\psi_+ - |+\rangle). \quad (\text{B.6})$$

We obtain

$$\beta = \frac{g}{2(1-\zeta)}, \quad \gamma = \frac{g}{4}, \quad \delta = \frac{g}{2(1+\zeta)}. \quad (\text{B.7})$$

The analysis for $|-\rangle$ is analogous and leads to $\psi_- = TP_z\psi_+$. Once the degeneracy is lifted, the ground state should be an eigenstate of TP_z , hence it should be of the form

$$\frac{1}{\sqrt{2}}(\psi_+ \pm \psi_-). \quad (\text{B.8})$$

We are now in the position to compute correlation functions on the ground state. For the local magnetization, we obtain

$$\begin{aligned} m_i &= 0 \quad \text{for } i = 2, \dots, L-1 \\ m_1 &= -m_L = \delta^2 - \beta^2 = -\frac{g^2\zeta}{(1-\zeta^2)^2}. \end{aligned} \quad (\text{B.9})$$

This result shows the the ground state does not show a local magnetization, except at the boundaries. For $i \neq 1, L$, the local magnetization $m(i)$ vanishes as in the zero-field case. The applied field ζ is too small to destabilize the low-energy state. We can analogously compute the correlation function $G(i, j)$:

$$G(1, L) = 1 - 2\beta^2 - 2\delta^2 = 1 - \frac{(1+\zeta^2)g^2}{(1-\zeta^2)^2}, \quad (\text{B.10})$$

$$G(i, L) = G(1, i) = 1 - \beta^2 - \delta^2 - 2\gamma^2 = 1 - \frac{(5 + 2\zeta^2 + \zeta^4)g^2}{8(1-\zeta^2)^2}, \quad (\text{B.11})$$

$$G(i, j) = 1 - 4\gamma^2 = 1 - g^2/4 = m_0^2 + O(g^3), \quad (\text{B.12})$$

where $1 < i \neq j < L$. Except on the boundaries, the correlation function is equal to the square of the bulk magnetization m_0^2 , as in the zero-field case.

Appendix B.2. Large-field kink phase

Let us now consider the large-field region in which the ground state is $(L-1)$ degenerate and the relevant states are the kink states (B.2). The degeneracy is lifted when H_g is included. The full Hamiltonian restricted to the subspace spanned by the kink states has the form (we write it for $L=5$)

$$H = \begin{pmatrix} E_0 & -g & 0 & 0 \\ -g & E_0 & -g & 0 \\ 0 & -g & E_0 & -g \\ 0 & 0 & -g & E_0 \end{pmatrix}, \quad (\text{B.13})$$

where $E_0 = -(L-3) - 2\zeta$. The eigenvalues and eigenvectors of this matrix have been computed in Appendix A.1. There are $L-1$ energy states

$$E_m = E_0 + 2g \cos \frac{\pi m}{L}, \quad (\text{B.14})$$

with $m = 1, \dots, L-1$. The ground state corresponds to $m = L-1$. The corresponding eigenfunctions are

$$|m\rangle = \sqrt{\frac{2}{L}} \sum_{j=1}^{L-1} (-1)^j \sin k_m j |j\rangle_k, \quad (\text{B.15})$$

with $k_m = \pi m/L$. Using this expression, we can compute the average of $\sigma_i^{(1)}$. For the average on state m , we obtain

$$\begin{aligned} \langle m | \sigma_1^{(1)} | m \rangle &= -\langle m | \sigma_L^{(1)} | m \rangle = -1, \\ \langle m | \sigma_i^{(1)} | m \rangle &= \frac{2}{L} \sum_{j < i} \sin^2 k_m j - \frac{2}{L} \sum_{j \geq i} \sin^2 k_m j, \end{aligned} \quad (\text{B.16})$$

where $2 \leq j \leq L-1$. If we now consider the ground state, in the large- L limit, we can rewrite Eq. (B.16) as

$$m_j = -1 + \frac{2j}{L} - \frac{1}{\pi} \sin \frac{2\pi j}{L}. \quad (\text{B.17})$$

If we define $x = i - L/2$ and $\ell = L/2$ we obtain the more symmetric form

$$m(x) = \frac{x}{\ell} + \frac{1}{\pi} \sin \frac{\pi x}{\ell}. \quad (\text{B.18})$$

Analogously, we can compute the correlation function. We obtain

$$\begin{aligned} \langle m | \sigma_1^{(1)} \sigma_L^{(1)} | m \rangle &= -1, \\ \langle m | \sigma_1^{(1)} \sigma_j^{(1)} | m \rangle &= -\langle m | \sigma_j^{(1)} | m \rangle, \\ \langle m | \sigma_L^{(1)} \sigma_j^{(1)} | m \rangle &= \langle m | \sigma_j^{(1)} | m \rangle, \\ \langle m | \sigma_j^{(1)} \sigma_k^{(1)} | m \rangle &= \frac{2}{L} \sum_{i < j} \sin^2 k_m i - \frac{2}{L} \sum_{j \leq i < k} \sin^2 k_m i + \frac{2}{L} \sum_{i > k} \sin^2 k_m i, \end{aligned} \quad (\text{B.19})$$

where $2 \leq j < k \leq L-2$. Focusing again on the ground state and taking the limit $L \rightarrow \infty$, if $x = j - L/2$, $y = k - L/2$, we obtain

$$G(j, k) = 1 - \frac{|x - y|}{\ell} - \frac{1}{\pi} \left| \sin \frac{\pi x}{\ell} - \sin \frac{\pi y}{\ell} \right| = 1 - |m(j) - m(k)|. \quad (\text{B.20})$$

Appendix B.3. Intermediate case

We should now discuss the behavior of the system in the intermediate case in which kink states and ferromagnetic states are degenerate. For $g = 0$ this case corresponds to $\zeta = 1$. As discussed in Sec. 6, when the g dependent term is added, the intermediate case corresponds to $\zeta_c = \sqrt{1-g} \approx 1 - g/2$. Therefore, to discuss the intermediate case, we set $\zeta = 1 - g/2$ and consider the model restricted to the $(L+1)$ subspace spanned by $|0\rangle = |-\rangle$, $|i\rangle_k$ ($k = 1, \dots, L-1$), $|L\rangle = |+\rangle$. If $E_0 = -(L-3) - 2\zeta_c$ is the energy of the kink states, the Hamiltonian can be written as (here $L = 4$)

$$H = \begin{pmatrix} E_0 - g & -g & 0 & 0 & 0 \\ -g & E_0 & -g & 0 & 0 \\ 0 & -g & E_0 & -g & 0 \\ 0 & 0 & -g & E_0 & -g \\ 0 & 0 & 0 & -g & E_0 - g \end{pmatrix}. \quad (\text{B.21})$$

The eigenvalues can be computed using the results of Appendix A.1. Indeed, H has the same form as matrix \tilde{A} defined in Eq. (A.14). Since $\delta = -g$, the secular equation (A.17) becomes

$$(1 + \cos k) \frac{\sin k(L+1)}{\sin k} = 0, \quad (\text{B.22})$$

which implies

$$k = \frac{\pi m}{L+1} \quad m = 1, \dots, L+1. \quad (\text{B.23})$$

As the energy of each mode is given by $E = E_0 + 2g \cos k$, the ground state is obtained by taking $k = \pi$. The ground-state energy is $E_0 - 2g$ and the corresponding eigenvector is simply

$$|GS\rangle = \frac{1}{\sqrt{L+1}} \sum_{j=0}^L |j\rangle. \quad (\text{B.24})$$

It is easy to compute the local magnetization and the correlation function. We find

$$m(i) = -1 + \frac{2i}{L+1}, \quad (\text{B.25})$$

which shows that $m(i)$ varies linearly between $1 - 2/(L+1)$ and $-1 + 2/(L+1)$. If we set, as usual, $x = i - L/2$ and $\ell = L/2$ we obtain in the large- L limit

$$m(i) = \frac{x}{\ell}. \quad (\text{B.26})$$

The two-point correlation function is also easily computed

$$G(i, j) = 1 - \frac{2|i-j|}{L+1} = 1 - |m(i) - m(j)|. \quad (\text{B.27})$$

Appendix B.4. Crossover behavior

Let us now study the crossover behavior. We consider again the same basis as in Appendix B.3. The Hamiltonian becomes (here $L = 4$)

$$H = \begin{pmatrix} E_0 - g + 2g\zeta_s/L & -g & 0 & 0 & 0 \\ -g & E_0 & -g & 0 & 0 \\ 0 & -g & E_0 & -g & 0 \\ 0 & 0 & -g & E_0 & -g \\ 0 & 0 & 0 & g & E_0 - g + 2g\zeta_s/L \end{pmatrix}. \quad (\text{B.28})$$

The secular equation is obtained by using the results of Appendix A.1, Eq. (A.17). We set $b = -g$, $d = E_0$, $e = E_0 - g + 2g\zeta_s/L$, and $E = E_0 + 2g \cos k$. Since $\delta = 2\zeta_s/L - 1$, we obtain

$$\frac{4\zeta_s}{L} \left(1 - \frac{\zeta_s}{L}\right) \sin k(L+2) + 2 \left(1 - \frac{2\zeta_s}{L}\right) \left[1 + \left(1 - \frac{2\zeta_s}{L}\right) \cos k\right] \sin k(L+1) = 0. \quad (\text{B.29})$$

In the kink phase in which $\zeta_s > 0$, k varies between $k = \pi$ for $\zeta_s = 0$ and $k = \pi - \pi/L$ for $\zeta_s \rightarrow \infty$. Hence, we write $k = \pi - z/L$. Expanding the secular equation to order $1/L^2$ we obtain

$$4\zeta_s z + (4\zeta_s^2 - z^2) \tan z = 0, \quad (\text{B.30})$$

which coincides with Eq. (83). The solutions of this equation either solve $\tan z/2 = 2\zeta_s/z$ or $\tan z/2 = -z/(2\zeta_s)$. The ground state corresponds to the lowest value of z that is a solution of Eq. (B.30), hence it satisfies $\tan z/2 = 2\zeta_s/z$. Note the limiting values:

$$\begin{aligned} z &\approx 2\sqrt{\zeta_s} && \text{for } \zeta_s \rightarrow 0, \\ z &\approx \pi(1 - 1/\zeta_s) && \text{for } \zeta_s \rightarrow +\infty. \end{aligned} \quad (\text{B.31})$$

We wish now to compute the ground-state eigenfunction, which we express as $(\alpha_1, \dots, \alpha_{L+1})$ in the basis $|j\rangle$, $j = 0, \dots, L$, defined in Appendix B.3. If $\bar{k} = \pi - k = z/L$, the coefficients satisfy the relations

$$\alpha_1(2 \cos \bar{k} - 1 + 2\zeta_s/L) - \alpha_2 = 0, \quad (\text{B.32})$$

$$\alpha_{j-1} - 2\alpha_j \cos \bar{k} + \alpha_{j+1} = 0, \quad (\text{B.33})$$

$$\alpha_L - \alpha_{L+1}(2 \cos \bar{k} - 1 + 2\zeta_s/L) = 0. \quad (\text{B.34})$$

The solution of Eq. (B.33) is

$$\alpha_j = e_1 \cos \bar{k}j + e_2 \sin \bar{k}j. \quad (\text{B.35})$$

The constants e_1 and e_2 are fixed by condition (B.32) and by the normalization condition $\sum \alpha_j^2 = 1$. In the large- L limit these two conditions give

$$e_1 = z \sqrt{\frac{2}{(4\zeta_s^2 + 4\zeta_s + z^2)L}}, \quad (\text{B.36})$$

$$e_2 = 2\zeta_s \sqrt{\frac{2}{(4\zeta_s^2 + 4\zeta_s + z^2)L}}. \quad (\text{B.37})$$

We can now compute $m(i)$ and $G(i, j)$. For the local magnetization we have

$$m(i) = \alpha_1^2 - \alpha_{L+1}^2 + \sum_{1 < j \leq i} \alpha_j^2 - \sum_{i < j \leq L} \alpha_j^2. \quad (\text{B.38})$$

In the large- L limit, using $\tan z/2 = 2\zeta_s/z$, we obtain

$$m(i) = \frac{z}{z + \sin z} \left(\frac{1}{z} \sin \frac{zx}{\ell} + \frac{x}{\ell} \right), \quad (\text{B.39})$$

where $x = i - L/2$, $\ell = L/2$. Note that the prefactor guarantees that $m(i)$ is equal to ± 1 at the two boundaries. We can also compute the correlation function, which satisfies the relation

$$G(i, j) = 1 - |m(i) - m(j)|. \quad (\text{B.40})$$

Correspondingly, we obtain

$$\frac{\chi}{L} = \frac{z^2 - 2 + 2 \cos z + 2z \sin z}{2z(z + \sin z)}, \quad (\text{B.41})$$

and

$$\frac{\xi^2}{L^2} = \frac{z^4 + 24 + 12(z^2 - 2) \cos z + 4z(z^2 - 6) \sin z}{48z^2(z^2 - 2 + 2 \cos z + 2z \sin z)}. \quad (\text{B.42})$$

Let us finally consider $n_s(i)$ defined in Eq. (97). For $g \rightarrow 0$, $n_h = 1/2$, so that $n_s(i) = \langle \sigma_i^{(3)} \rangle / 2$. Using the definition we obtain

$$n_s(i) = \alpha_i \alpha_{i+1}. \quad (\text{B.43})$$

Substituting the explicit expression of α_i and using $\tan z/2 = 2\zeta_s/z$, we find

$$Ln_s(i) = \frac{z}{(z + \sin z)} \left(1 + \cos \frac{zx}{\ell} \right). \quad (\text{B.44})$$

The above-reported results apply to the kink phase $\zeta_s \geq 0$. For $\zeta_s < 0$ the ground state is a localized state with $k = \pi + iu/L$, where u satisfies the equation

$$4\zeta_s u + (4\zeta_s^2 + u^2) \tanh u = 0. \quad (\text{B.45})$$

The solutions of this equation satisfy either $\tanh u/2 = -2\zeta_s/u$ or $\tanh u/2 = -u/(2\zeta_s)$. Since $E = E_0 - 2g \cosh u/L$, the ground state is obtained by considering the largest positive solution of the equation. It is then easy to prove that it satisfies $\tanh u/2 = -2\zeta_s/u$. The solution for $\zeta_s < 0$ is then obtained by analytic continuation of the results obtained for $\zeta_s > 0$. It is enough to replace z with $-iu$. We therefore obtain

$$m(i) = \frac{u}{u + \sinh u} \left(\frac{x}{\ell} + \frac{1}{u} \sinh \frac{ux}{\ell} \right), \quad (\text{B.46})$$

$$Ln_s(i) = \frac{u}{u + \sinh u} \left(1 + \cosh \frac{ux}{\ell} \right). \quad (\text{B.47})$$

Note that $u \approx -2\zeta_s$ for $\zeta_s \rightarrow -\infty$, so that

$$m(i) = \frac{\sinh 2\zeta_s x / \ell}{\sinh 2\zeta_s}, \quad Ln_s(i) = \frac{2\zeta_s \cosh 2\zeta_s x / \ell}{\sinh 2\zeta_s} \quad (\text{B.48})$$

in this limit.

References

- [1] S. Sachdev, *Quantum Phase Transitions*, (Cambridge Univ. Press, 1999).
- [2] H. Nishimori and G. Ortiz, *Elements of Phase Transitions and Critical Phenomena*, Chap. 10 (Oxford Univ. Press, Oxford, 2011).
- [3] E. Lieb, T. Schultz and D. Mattis, Two soluble models of an antiferromagnetic chain, *Ann. Phys. (NY)* **16**, 407 (1961).
- [4] S. Katsura, Statistical mechanics of the anisotropic linear Heisenberg model, *Phys. Rev.* **127**, 1508 (1962).
- [5] P. Pfeuty, The one-dimensional Ising model with a transverse field, *Ann. Phys. (NY)* **57**, 79 (1970).
- [6] E. Barouch and B. M. McCoy, Statistical Mechanics of the XY Model. II. Spin-Correlation Functions *Phys. Rev. A* **3**, 786 (1971)
- [7] M. Suzuki, Equivalence of the two-dimensional Ising model to the ground state of the linear XY-model, *Phys. Lett. A* **34**, 94 (1971).
- [8] N. Boccarda and G. Sarma, Does magnetic surface order exist?, *J. Physique Lett. (Paris)* **35**, 95 (1974).
- [9] G. G. Cabrera and R. Jullien, Universality of Finite-Size Scaling: the Role of the Boundary Conditions, *Phys. Rev. Lett.* **57**, 393 (1986); Role of boundary conditions in the finite-size Ising model, *Phys. Rev. B* **35**, 7062 (1987).
- [10] M. N. Barber and M. E. Cates, Effect of boundary conditions on the finite-size transverse Ising, *Phys. Rev. B* **36**, 2024 (1987).
- [11] M. Henkel, Finite-size scaling and universality in the spectrum of the quantum Ising chain. 1. Periodic and antiperiodic boundary conditions, *J. Phys. A* **20**, 995 (1987).
- [12] T. W. Burkhardt and I. Guim, Universal scaling form of the correlation length in Ising strips with periodic, free, fixed, and mixed boundary conditions, *Phys. Rev. B* **35**, 1799 (1987).
- [13] B. Berche and L. Turban, Inhomogeneous Ising chain in a transverse field. Finite-size scaling and asymptotic conformal spectrum, *J. Phys. A* **23**, 3029 (1990).
- [14] L. Turban and B. Berche, Surface magnetization of aperiodic Ising quantum chains, *Z. Phys. B* **92**, 307 (1993).
- [15] F. Igloi, I. Peschel, and L. Turban, Inhomogeneous systems with unusual critical behavior, *Adv. Phys.* **42**, 683 (1993)
- [16] D. Karevski, Surface and bulk critical behaviour of the XY chain in a transverse field, *J. Phys. A* **33**, L313 (2000).
- [17] N. S. Izmailian and C. K. Hu, Exact universal amplitude ratios for two-dimensional Ising models and a quantum spin chain, *Phys. Rev. Lett.* **86**, 5160 (2001).
- [18] I. Peschel, On the entanglement entropy for an XY spin chain, *J. Stat. Mech.: Theory Expt.* P12005 (2004).
- [19] N. Sh. Izmailian and C.-K. Hu, Boundary conditions and amplitude ratios for finite-size corrections of a one-dimensional quantum spin model, *Nucl. Phys. B* **808**, 613 (2009).
- [20] A. Dutta, U. Divakaran, D. Sen, B. K. Chakrabarti, T. F. Rosenbaum, and G. Aeppli, Quantum phase transitions in transverse field spin models: From Statistical Physics to Quantum Information, arXiv:1012.0653v3; A. Dutta, G. Aeppli, B. K. Chakrabarti, U. Divakaran, T. F. Rosenbaum and D. Sen, *Quantum Phase Transitions in Transverse Field Spin Models: From Statistical Physics to Quantum Information* (Cambridge University Press, Cambridge, 2015).
- [21] M. Campostrini, A. Pelissetto and E. Vicari, Finite-size scaling at quantum transitions, *Phys. Rev. B* **89**, 094516 (2014).
- [22] M. Campostrini, J. Nespola, A. Pelissetto, and E. Vicari, Finite-Size Scaling at First-Order Quantum Transitions, *Phys. Rev. Lett.* **113**, 070402 (2014).
- [23] M. Campostrini, A. Pelissetto, and E. Vicari, Quantum transitions driven by one-bond defects in quantum Ising rings, *Phys. Rev. E* **91**, 042123 (2015).
- [24] S. Dietrich, Wetting Phenomena, in *Phase Transitions and Critical Phenomena*, vol. 12, edited by

- C. Domb and J. L. Lebowitz (Academic, London, 1988).
- [25] J. O. Indekeu, Line tension at wetting, *Int. J. Mod. Phys.* **8**, 309 (1994).
 - [26] D. Bonn and D. Ross, Wetting transitions, *Rep. Progr. Phys.* **64**, 1085 (2001).
 - [27] K. Binder, D. P. Landau, and M. Müller, Monte Carlo studies of wetting, interface localization and capillary condensation, *J. Stat. Phys.* **110**, 1411 (2003).
 - [28] A. Y. Kitaev, Unpaired Majorana fermions in quantum wires, *Phys. Usp.* **44**, 131 (2001).
 - [29] J. Alicea, New directions in the pursuit of Majorana fermions in solid state systems, *Rep. Prog. Phys.* **75**, 076501 (2012).
 - [30] U. Schollwöck, The density-matrix renormalization group, *Rev. Mod. Phys.* **77**, 259 (2005).
 - [31] C.R. Laumann, R. Moessner, A. Scardicchio, and S. L. Sondhi, Quantum Adiabatic Algorithm and Scaling of Gaps at First-Order Quantum Phase Transitions, *Phys. Rev. Lett.* **109**, 030502 (2012)
 - [32] *Entanglement Entropy in Extended Systems*, edited by P. Calabrese, J. Cardy, and B. Doyon, *J. Phys. A* **42**, 500301 (2009).
 - [33] D. B. Abraham, Solvable model with a roughening transition for a planar Ising ferromagnet, *Phys. Rev. Lett.* **44**, 1165 (1980).
 - [34] H. Nakanishi and M. E. Fisher, Multicriticality of wetting, prewetting, and surface transitions, *Phys. Rev. Lett.* **49**, 1565 (1982).
 - [35] A. Ciach, Correlation functions in the solid-on-solid model of the fluctuating interface, *Phys. Rev. B* **34**, 1932 (1986).
 - [36] A. Ciach and J. Stecki, Scaling in the solid-on-solid interface, *J. Phys. A* **20**, 5619 (1987).
 - [37] V. Privman and N. M. Švrakič, Finite-size scaling for the restricted solid-on-solid model of the two-dimensional wetting transition, *Phys. Rev. B* **37**, 3713 (1988).
 - [38] A. O. Parry and R. Evans, Influence of wetting on phase equilibria: A novel mechanism for critical-point shifts in films, *Phys. Rev. Lett.* **64**, 439 (1990).
 - [39] A. O. Parry, R. Evans, and D. B. Nicolaides, Long-ranged surface perturbations for confined fluids, *Phys. Rev. Lett.* **67**, 2978 (1991).
 - [40] J. Stecki, A. Maciolek, and K. Olaussen, Magnetization profiles of the planar fluctuating interface in a $d = 2$ Ising strip, *Phys. Rev. B* **49**, 1092 (1994).
 - [41] A. Maciolek and J. Stecki, $d = 2$ Ising strip with two surface fields solved using the transfer-matrix method, *Phys. Rev. B* **54**, 1128 (1996).
 - [42] A. Maciolek, Magnetization profiles for a $d = 2$ Ising strip with opposite surface fields, *J. Phys. A* **29**, 3837 (1996).